

# The Mars Global Surveyor Ka-Band Link Experiment (MGS/KaBLE-II)

D. Morabito,<sup>1</sup> S. Butman,<sup>1</sup> and S. Shambayati<sup>1</sup>

*The Mars Global Surveyor (MGS) spacecraft, launched on November 7, 1996, carries an experimental space-to-ground telecommunications link at Ka-band (32 GHz) along with the primary X-band (8.4-GHz) downlink. The signals are simultaneously transmitted from a 1.5-m-diameter parabolic antenna on MGS and received by a beam-waveguide (BWG) research and development (R&D) 34-meter antenna located in NASA's Goldstone Deep Space Network (DSN) complex near Barstow, California. This Ka-band link experiment (KaBLE-II) allows the performances of the Ka-band and X-band signals to be compared under nearly identical conditions. The two signals have been regularly tracked during the past 2 years. This article presents carrier-signal-level data ( $P_c/N_o$ ) for both X-band and Ka-band acquired over a wide range of station elevation angles, weather conditions, and solar elongation angles. The cruise phase of the mission covered the period from launch (November 7, 1996) to Mars orbit capture (September 12, 1997). Since September 12, 1997, MGS has been in orbit around Mars. The measurements confirm that Ka-band could increase data capacity by at least a factor of three (5 dB) as compared with X-band. During May 1998, the solar corona experiment, in which the effects of solar plasma on the X-band and Ka-band links were studied, was conducted. In addition, frequency and difference frequency ( $f_x - f_{Ka}/3.8$ ), ranging, and telemetry data results are presented.*

*MGS/KaBLE-II measured signal strengths (for 54 percent of the experiments conducted) that were in reasonable agreement with predicted values based on pre-flight knowledge, and frequency residuals that agreed between bands and whose statistics were consistent with expected noise sources. For passes in which measured signal strengths disagreed with predicted values, the problems were traced to known deficiencies, for example, equipment operating under certain conditions, such as a cold Ka-band solid-state power amplifier (SSPA) temperature, and a degraded response at higher frequencies in certain modes. These efforts had continued with Deep Space 1 (DS1), launched in October 1998, which also emits Ka-band and X-band signals.*

## I. Introduction

The capability to communicate across interplanetary distances has grown by many orders of magnitude since the advent of space exploration 40 years ago. About 19 dB of the improvement (a factor of 76)

---

<sup>1</sup> Communications Systems and Research Section.

results from increased antenna gain, which scales as the square of frequency. Since 1959, there has been an 8.8-fold increase in the radio frequency—from L-band (0.96 GHz) to X-band (8.4 GHz) in 1977, the primary downlink frequency today [1]. A shift to Ka-Band (32 GHz) is projected to add another 5 to 6 dB. The increase in antenna gain with Ka-band is actually 11.6 dB relative to X-band; however, atmospheric and amplifier noise and attenuation diminish that by 4 to 5 dB. A further loss of 1.5 to 2 dB is attributed to DSN antenna imperfections that are less significant at X-band. In terms of spacecraft mass and power savings, the anticipated 5- to 6-dB improvement requires Ka-band transmitters that are no more massive nor less efficient than those at X-band.

To determine if Ka-band will be viable operationally requires that performance data be gathered under varying operating conditions—with weather and over a wide DSN antenna elevation-angle range and in different spacecraft modes over a statistically significant period. This is accomplished by Mars Global Surveyor Ka-Band Link Experiment (MGS/KaBLE-II), which transmits in both bands, as depicted in Fig. 1(a). The flight trajectory of MGS is displayed in Fig. 1(b).

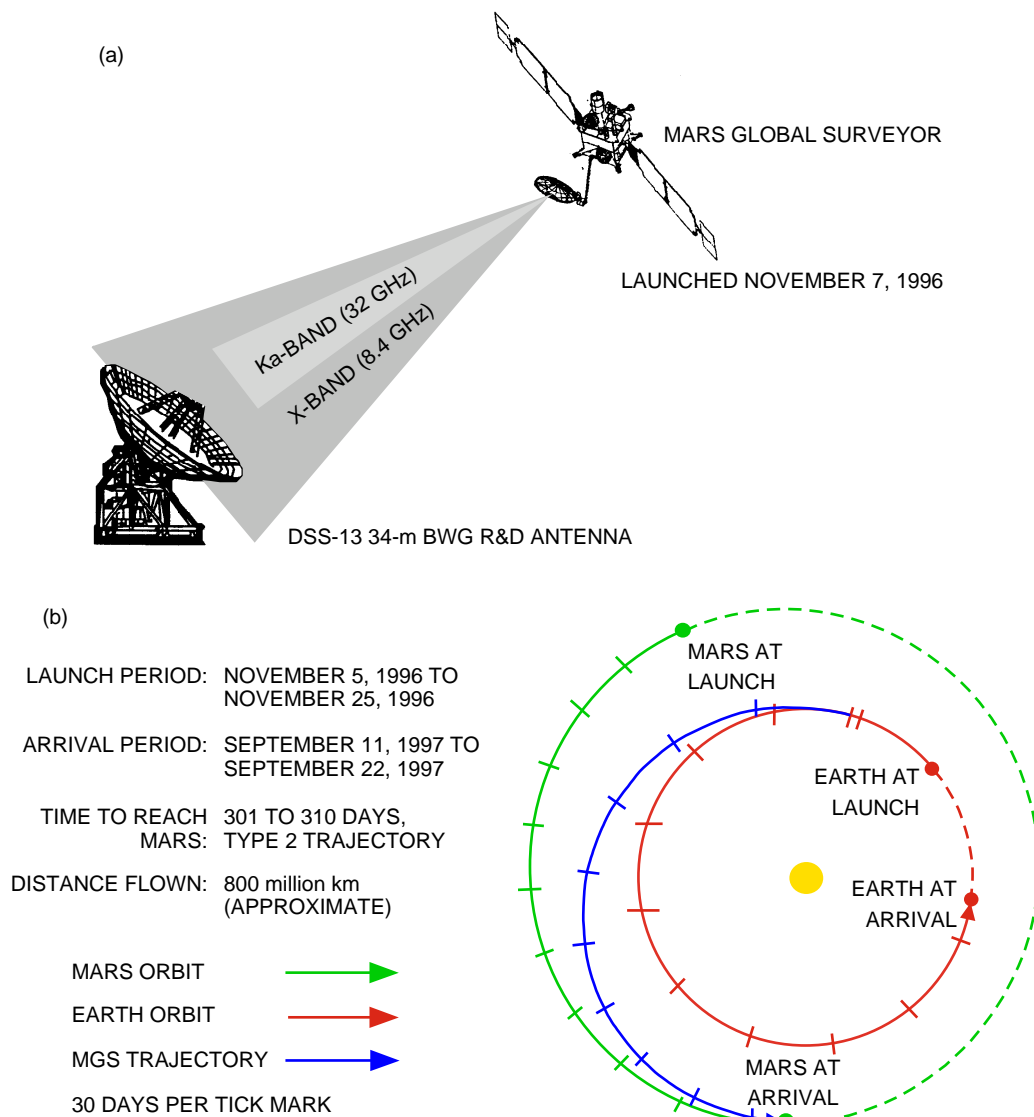


Fig. 1. Depictions of (a) the X-/Ka-band experiment and (b) the MGS flight trajectory.

The MGS/KaBLE-II signal-level and frequency data presented in this article were accumulated between December 1996 and December 1998 (see Tables 2 and 3). End-to-end telemetry and ranging demonstrations were successfully conducted during April and May 1997. The MGS high-gain antenna (HGA) pointed to within 0.10 deg, and the DSS-13 ground antenna had a tracking error of less than 1 mdeg for most tracks.

The signals from MGS also have been tracked through the solar conjunction period of May 1998 in order to observe propagation effects through the solar plasma. The increased Ka-band advantage relative to X-band for passes conducted angularly near the Sun was demonstrated.

MGS/KaBLE-II also has been used to check out DSS 25, a new 34-m station, in order to prepare to support the X-band and Ka-band downlinks on the Cassini and DS1 missions. This article describes the spacecraft, ground system, ground operations, and data analysis results. Initial reports of this work were presented in [2] and [3].

## II. Spacecraft Configuration

The MGS mission was conceived as a low-cost, rapid replacement for Mars Observer (MO), which was lost on August 18, 1993. MO carried the original KaBLE, which functioned well within its limitations [4]. However, with an effective isotropic radiated power (EIRP) of 50 dBm, the Ka-band signal on MO would have been too weak to track at Mars' distance, and at 33.68 GHz, its frequency was outside the 31.8- to 32.3-GHz band allocated for deep space.

The MGS spacecraft contract awarded to Lockheed Martin Astronautics Co. (LMA) in June of 1994 included a functional equivalent of MO/KaBLE. However, the need now was to (1) maximize EIRP, (2) transmit in the DSN frequency band, and (3) be coherent with the X-band downlink. The challenge was to develop and deliver the enhanced KaBLE-II in 15 months, from October 1994 to January 1996. The spacecraft, therefore, was not accessible to non-mission-critical changes.

The design evolved by LMA and JPL is as shown in Fig. 2. A low-power sample of the X-band downlink from the transponder is upconverted to 32 GHz, amplified to 1 W, and radiated from the dual X-/Ka-band HGA. The 1-W solid-state power amplifier (SSPA) adapted from another LMA program has an efficiency of 10 percent. The spare MO HGA X-band feed was replaced by the dual-frequency

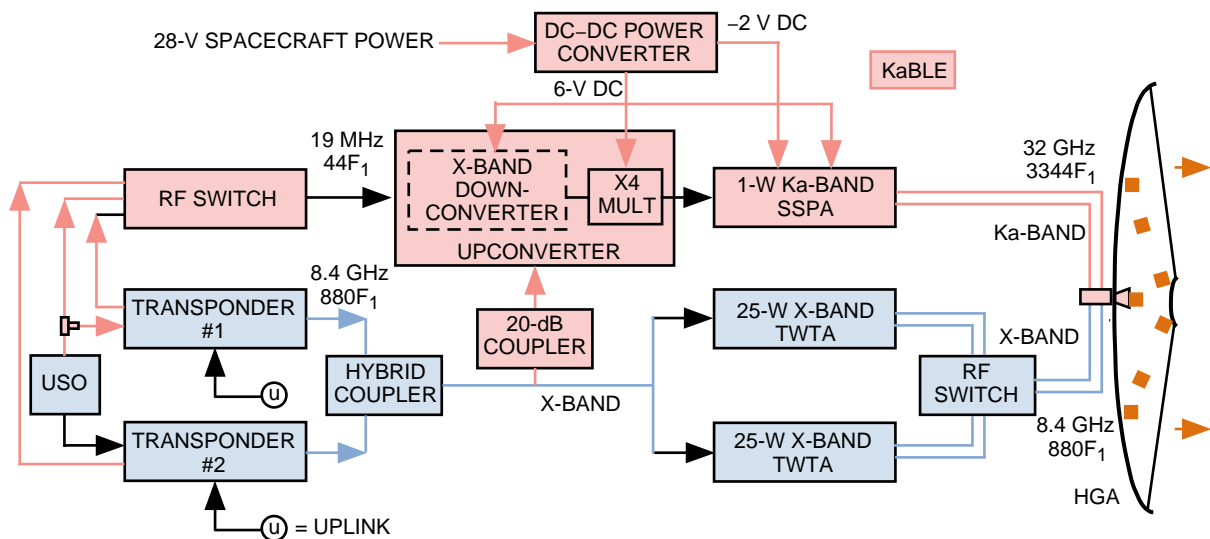


Fig. 2. The MGS/KaBLE-II spacecraft telecommunications system.

X-/Ka-band horn, developed by LMA [5]. Figure 3 shows the MGS HGA along with the X-band and Ka-band gain versus angle off boresight. Figure 4 displays the traveling-wave tube amplifier (TWTA) enclosure, which also houses the KaBLE-II electronics hardware. The X-band signal is amplified by one of two 25-W TWTAs, which also feed to the HGA.

The upconverter, shown in Fig. 2, first downconverts the 8.42 GHz (880 f1) to 8 GHz (836 f1), which then is multiplied by the X4 multiplier, producing the 32-GHz (3344 f1) Ka-band frequency. As a result, the Ka-band phase modulation is four times the X-band phase modulation. The downconverter and X4 multiplier were made for JPL by Milliwave Inc. The DC-DC converter was manufactured by Modular Devices Incorporated. With the exception of the RF switch, all KaBLE-II components and X-band power components are located in the TWTA enclosure mounted on the HGA, as depicted in Fig. 4. The KaBLE-II equipment draws 20 W of DC power and has a mass of 1 kg.

The Ka-band downlink is coherent with the X-band downlink only if the downconverter is driven by the same frequency source as is the X-band downlink. The frequency source selection is performed by the RF switch, which can be commanded to select voltage-controlled oscillator 1 (VCO1), VCO2 or the ultra-stable oscillator (USO), or OFF. This creates several possible Ka-band frequencies for each

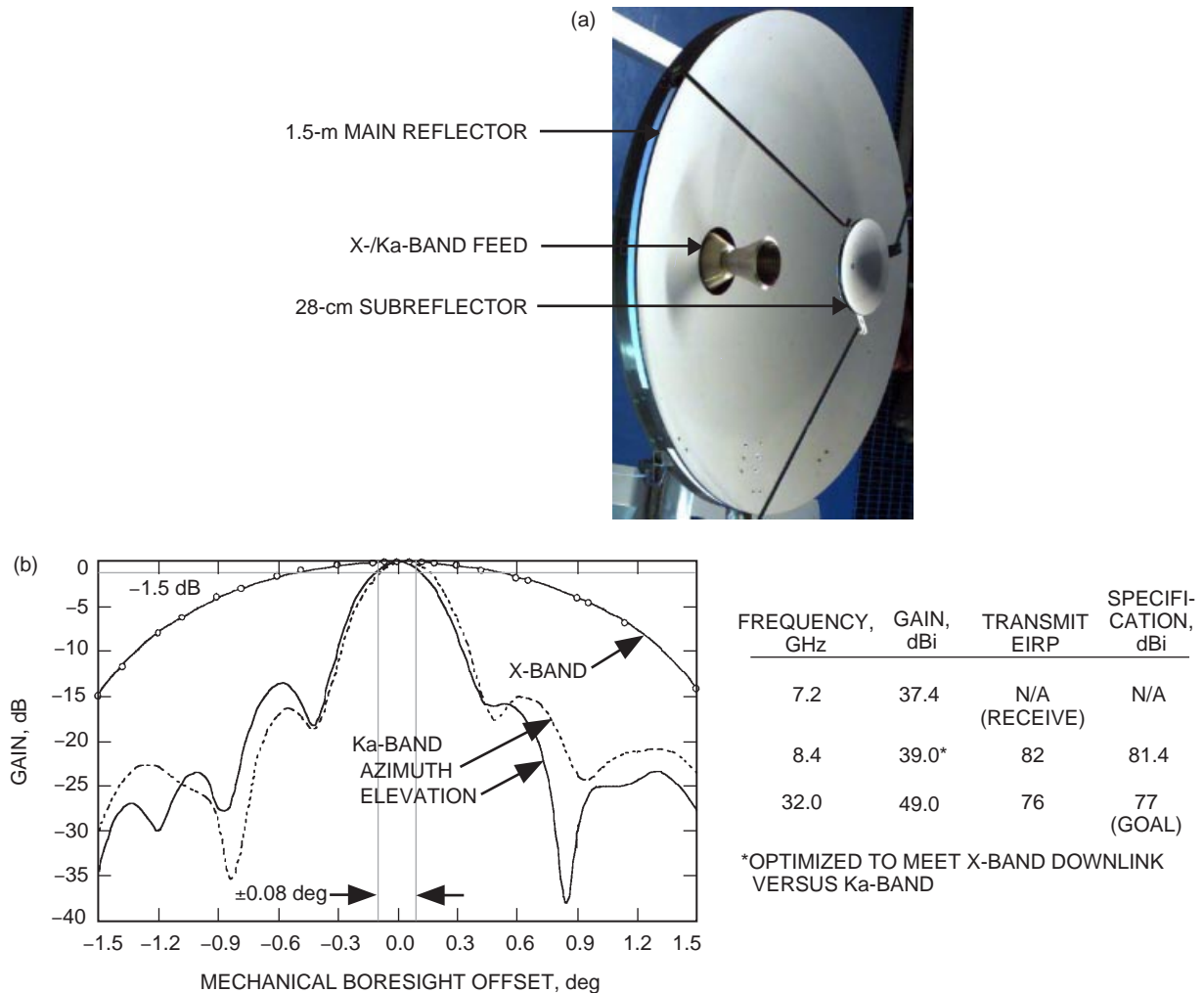


Fig. 3. The MGS (a) HGA and (b) X-/Ka-band gain patterns.

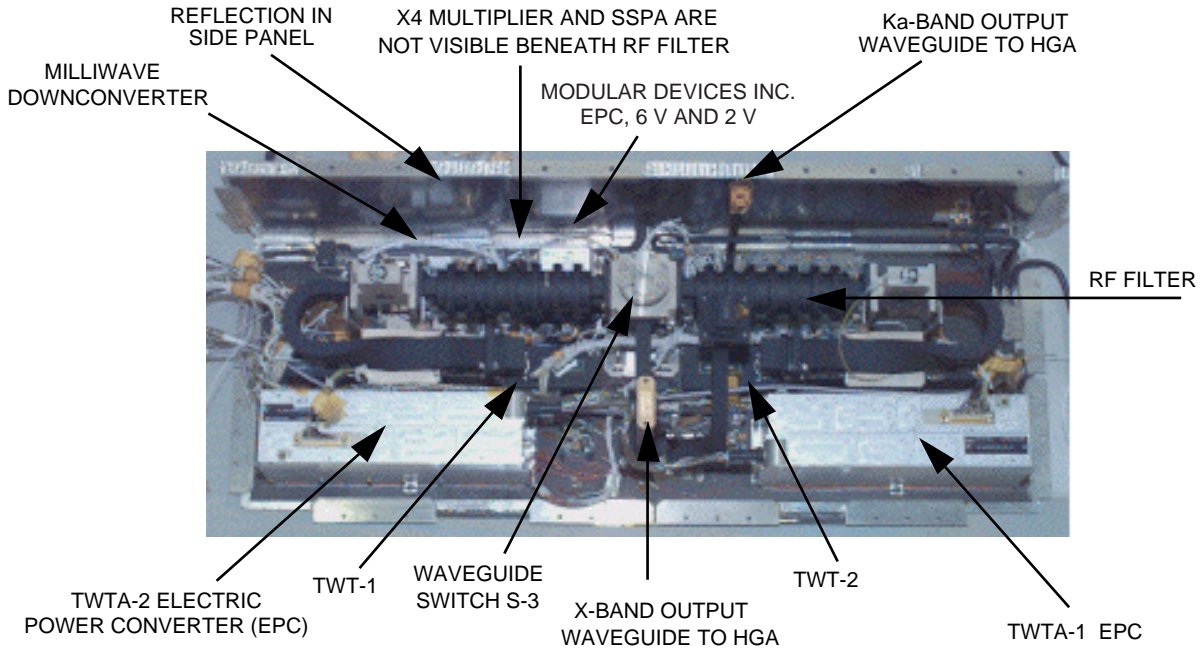


Fig. 4. MGS spacecraft telecommunications electronics hardware.

X-band frequency. The Ka-band frequency can be either coherent with the X-band downlink or a hybrid combination of the USO- and VCO1- or VCO2-derived frequencies. The possibilities are given by

$$f_{Ka} = 4f_X - 0.2f_S \quad (1)$$

where  $f_X$  is the X-band downlink frequency and  $f_S$  is the X-band downlink frequency that would result from the oscillator selected by the switch (nominally the USO-referenced downlink is at 8.4231 GHz and those of the VCOs are at 8.4177 GHz). A VCO could be locked to the uplink or be free running, which further complicates the Ka-band downlink modes and predict-generation process.

Various anomalous behaviors that were known from the prelaunch testing activities were observed during flight.<sup>2</sup> These KaBLE-II downconverter anomalies, which occurred under different operating modes, primarily involved degradation of carrier-signal power with low SSPA temperature (below 30 deg C), high RF frequency, high subcarrier frequency, and high modulation index. These will be discussed in a later section.

### III. Ground System Configuration

The ground station used to acquire the MGS/KaBLE-II data is DSS 13 (see Fig. 5), a 34-m beam-waveguide (BWG) antenna located at the NASA Goldstone Deep Space Communications Complex near Barstow, California. DSS 13 is a research and development (R&D) antenna that was built as a prototype for the evolving DSN BWG subnet. This antenna incorporates a series of mirrors inside beam-waveguide tubes that channel the energy into a subterranean pedestal room (see Fig. 6), which provides a stable environment for the feed and electronics equipment. Such an arrangement provides easy access to multiple feeds located at different positions on a circular ring, resulting in lower maintenance costs as compared

<sup>2</sup>A. McMechen, "MGS Spacecraft Final X- and Ka-Band Spectrums," Lockheed Martin Interoffice Memorandum TS-0896-01 (internal document), Lockheed Martin Astronautics Flight Systems, Denver, Colorado, August 12, 1996.

with non-BWG antennas, which usually have a single package in a feed cone mounted on the main reflector surface. In addition, since the feed packages are located inside the subterranean room, there is less susceptibility to weather effects.

Figure 7 illustrates a block diagram of the DSS-13 station configuration used for conducting the KaBLE-II experiments. A small amount of new development was required since the MO/KaBLE experiments. On the antenna, RF mirrors guide and focus the RF energy onto a feed horn on a low-noise amplifier (LNA). The Ka-band monopulse receiver used for the LNA enabled the antenna to autotrack the spacecraft to 1-mdeg accuracy. The DSS-13 antenna efficiency is 43 to 57 percent depending on the elevation and feed package [6]. The system operating noise temperature also is elevation dependent and changes with weather.



**Fig. 5. DSS 13, a 34-m R&D beam-waveguide antenna.**

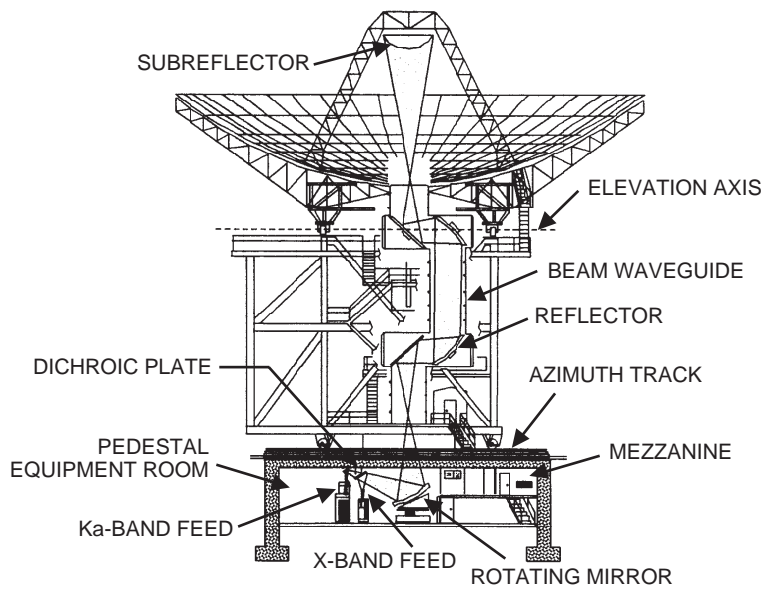


**Fig. 6. The DSS-13 reflectors, mirrors, optics paths, and MGS/KaBLE-II feed packages.**

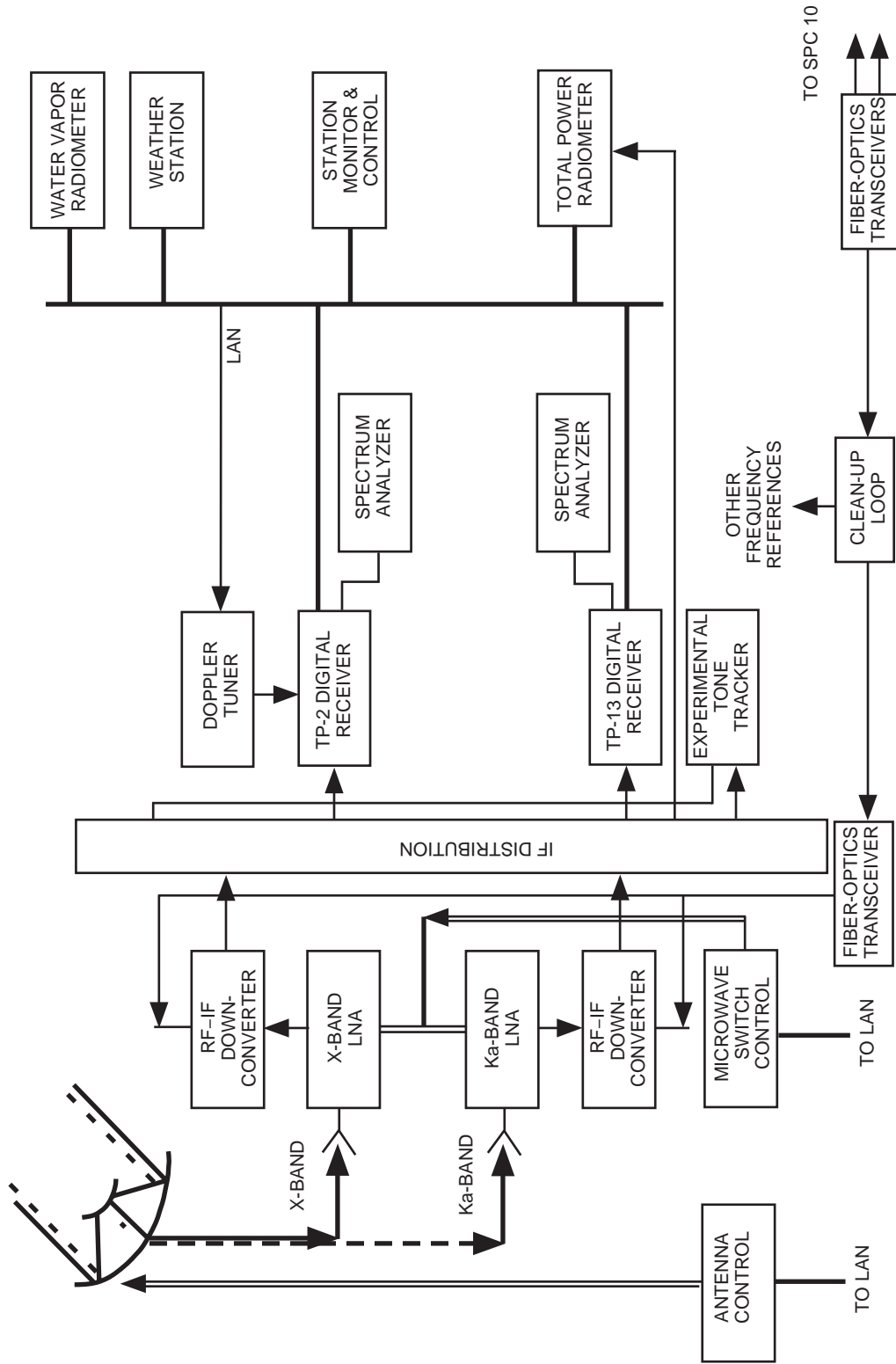


Fig. 7. DSS-13 ground-station configuration for MGS/KaBLE-II.

## A. Monopulse Feed–LNA Package

With the exception of the first 2 months of tracking, the monopulse package was used to acquire the Ka-band data. For data collected using the array feed (for the first 2 months of tracking), the reader is referred to [7] for a description of that system.

The monopulse package generates a low-noise sum-channel signal and an error-channel signal. The signal from the sum channel is downconverted to 300 MHz IF, filtered, and distributed for processing by other equipment. The LNA package, which consists of microwave components and high-electron-mobility-transistor (HEMT) amplifiers, is cryogenically cooled. The total DSS-13 system-noise operating temperature using the monopulse LNA is about 75 K at zenith during relatively clear weather conditions.

When the antenna is pointed directly at the spacecraft, the signals arrive along the axis of the horn and only the HE11 mode is generated. When the antenna is mispointed, signals arrive off axis and TE21 modes are generated. A piece of circular waveguide surrounded by eight directional couplers detect the TE21 mode signals. The direction of the pointing error determines the distribution of energy among the eight couplers. The error-channel signal is generated by combining the eight coupler outputs in a waveguide combining network.

When the antenna is mispointed, the voltage ratio of the error channel divided by the sum channel is proportional to the pointing error. The direction of the pointing error is proportional to the phase difference between the error and the sum-channel signals. The amplitude and phase of the signal in the sum channel and the error channel are extracted from noise by narrowband fast Fourier transforms (FFTs) and are used to calculate pointing error. The contribution of spacecraft Doppler is removed in the downconversion process by programming one of the local oscillators (the Doppler tuner developed for MO/KaBLE) with the use of a special set of frequency predicts in the form of Chebychev polynomials (see Section IV.A).

During experiments, the antenna is initially pointed using spacecraft pointing predicts generated from PG13, a Navigation and Flight Mechanics Section predict-generation program that reads input trajectory and ephemeris files. The monopulse computer determines the pointing error based on FFTs and corrects the antenna pointing by sending elevation and cross-elevation offsets to the antenna every 5 seconds. At each update time, the antenna pointing is corrected by about 0.4 times the measured pointing error. The monopulse antenna-pointing system is described in [8].

Figure 8 displays how the monopulse-determined pointing corrections (relative to the previous correction) relate to received carrier signal-to-noise ratio (SNR) for 120 passes conducted between February 1997 and May 1998. During the vast majority of the tracks, for Ka-band signal levels of between 13 and 43 dB-Hz, the monopulse tracking-system pointing errors were less than about 1 mdeg. During high gusty wind conditions, the errors would increase for short periods within a track but were generally less than 2 mdeg. The errors and standard deviations of the pointing errors were found to be consistent with expected values given the received carrier SNRs. The absolute pointing accuracy of the calibrated monopulse system determined from boresight observations was found to be below 1 mdeg.

## B. Experimental Tone Tracker (ETT)

The experimental tone tracker<sup>3</sup> (ETT) is a digital phase-locked-loop receiver that was used to simultaneously track both X-band and Ka-band carrier signals during the MGS/KaBLE-II tracks at DSS 13. The analog signal inputs to the ETT are open-loop downconverted to baseband and then digitized. Digital phase-locked loops (PLLs) then are used to extract the SNR, frequency, and phase of the sinusoid in the passband. The baseband processor of the ETT uses 1-bit data samples and a 3-level stopping function.

---

<sup>3</sup> *Experimental Tone Tracker (ETT) Operators Manual*, Version 1.3 (internal document), Jet Propulsion Laboratory, Pasadena, California, October 6, 1995.

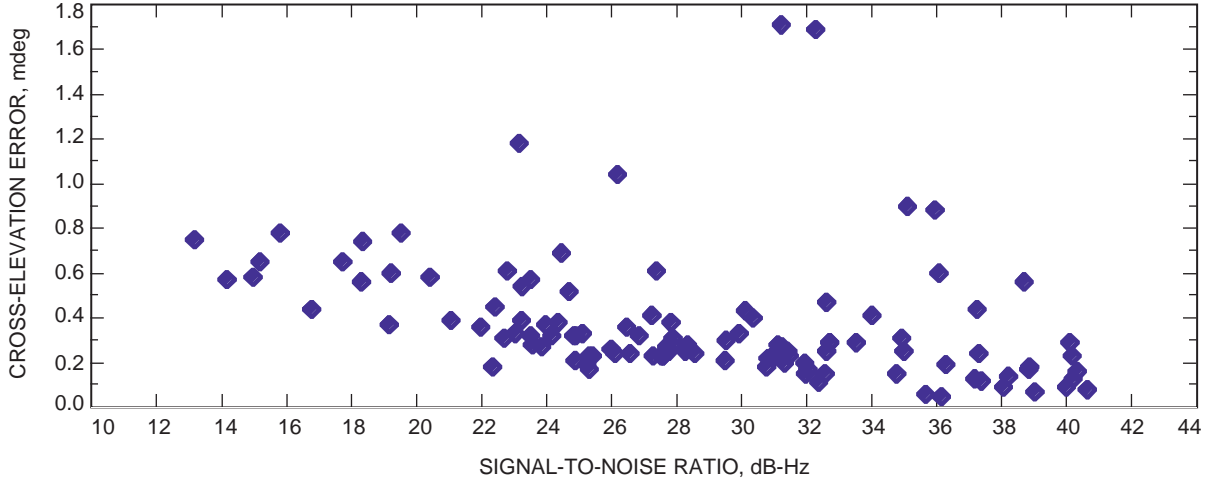


Fig. 8. The monopulse absolute value of cross-elevation pointing errors versus signal-to-noise ratio.

The ETT has been very reliable, with only two failures occurring out of 197 passes. A very useful feature of the ETT is that, when locked to a strong signal, it can be set to aid a weak coherent signal. This feature was used to detect Ka-band signals weakened by spacecraft antenna off pointing.

Once a signal is detected, the ETT processing utilizes a PLL that produces an estimate of the SNR ( $P_c/N_o$ ) in a 1-Hz bandwidth (BW) of the signal as well as the phase and frequency at the baseband. The ETT estimates of phase at 1-s sampled time tags are converted to frequency estimates by the KaBLE-II analysis software. These “locked” frequencies are written to files that are input to the STBLTY analysis software developed for radio science [9], producing frequency residuals, Allan deviation, reconstructed phase, and frequency/phase power density.

The measured  $P_c/N_o$  from the ETT (in a 16-MHz noise band) is effectively the received carrier signal strength divided by the thermal noise for a majority of passes when the spacecraft was far enough away from Earth that the temperature increase due to the spacecraft signal was negligible ( $\sim 0.1$  K). For earlier passes conducted shortly after launch when the spacecraft was near the Earth, this temperature increase was significant, and the measured  $P_c/N_o$  included a significant noise contribution due to the strong spacecraft signal.

### C. Telemetry-Processing Equipment

Two digital receiver processors, TP-2 and TP-13 [R&D versions of the DSN Block V receivers (BVRs)] were used to receive and demodulate the X- and Ka-band downlinks for several passes. TP-13 is dedicated to the X-band channel, TP-2 to the Ka-band channel. The receivers acquire and track carrier, subcarrier, and symbols.

The carrier and data channel signal-to-noise measurements using the TP-13 and TP-2 receivers were used to estimate the modulation indices for the X-band and Ka-band signals that were compared with preflight estimates (see Section V.A).

### D. Total Power Radiometer (TPR)

The total power radiometer (TPR) measures received signal and noise using 10- to 30-MHz filters. The TPR data are used to provide the thermal noise ( $N_o$ ) estimates to the  $P_c/N_o$  predictions. When the antenna is pointed a few degrees away from the spacecraft, the TPR measures the ground-station system noise directly. Radiometer calibrations are routinely conducted prior to every KaBLE-II track using ambient loads and noise diodes. However, on 97-318, it was discovered that the Ka-band ambient

load was improperly configured since the monopulse package was installed in early 1997. The problem was then corrected in the post-processing software. For passes conducted between 97-035 and 97-318, the radiometer power readings while on the noise diode were used to calibrate system gain.

### E. Ancillary Data

In addition to the data described above, water vapor radiometry (WVR) data and surface meteorological data also were acquired. These data were used to estimate the atmospheric noise and attenuation contributions in the link for the  $P_c/N_o$  predicts and for correlation with the  $P_c/N_o$  measurements. Figure 9 displays examples of atmospheric noise temperature at zenith measured by the WVR at 31.4 GHz and atmospheric noise measured by the TPR (while tracking the spacecraft signal), normalized to one air mass, using a “tip-curve” algorithm. The two cases include a clear-weather pass [97-182, Fig. 9(a)], where the two data sets follow each other within 1 K, and a rainy-weather pass [97-314, Fig. 9(b)], where the delay effect of huge rain cells passing through each system’s beam at different times is clearly apparent.

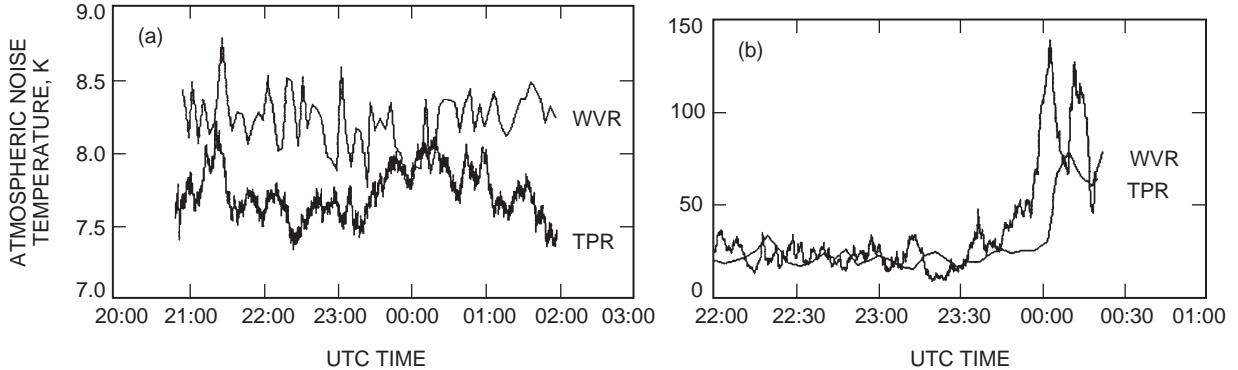


Fig. 9. Examples of WVR and TPR one-air-mass atmospheric noise temperatures: (a) clear weather, 97-182 and (b) rainy weather, 97-314.

## IV. MGS/KaBLE-II Operations

### A. Predicts Generation and Delivery

The task of routine spacecraft tracking at DSS 13, an R&D station, made necessary a special predicts-generation software package known as PG13. The basic requirements of PG13 were to provide time-tagged antenna-pointing predicts accurate to within 0.1 mdeg and frequency predicts for both X-band and Ka-band accurate to within  $\pm 100$  Hz (to fall within the acquisition range of the monopulse receiver system). Initial testing of the PG13 predicts package for MO/KaBLE experiments was described in [4]. For MGS/KaBLE-II, the procedures were significantly modified to handle MGS’s unique Ka-band/X-band ratios and hybrid frequency relationships. Thus, for input one-way and three-way X-band frequency predicts, additional utility routines were implemented to handle the various modes of expected Ka-band downlink frequency predicts.

Given  $f_{x(us0)}$  as the expected X-band one-way downlink referenced to the onboard USO, and  $f_{x(vco)}$  as the expected X-band three-way downlink referenced to an uplink generated from an operational DSN tracking station, the Ka-band downlink frequency predict sets that were supported are given in Table 1.

In addition, the X-band three-way predicts,  $f_{x(vco)}$ , could be referenced either to a single-frequency uplink during a pass (as was the case during the early cruise phase) or a ramped uplink at the operational DSN site that was designed to remove the uplink Doppler contribution leg such that the X-band uplink frequency into the spacecraft was near the best locked frequency (BLF) of the VCO. During the early phase of the mission, weekly phone calls to the DSN predict-generation team were necessary to obtain the uplink frequency used at the operational DSN uplink tracking station for each pass. For experiments conducted

during the orbital phase, the predict-generation software was modified to automatically generate three-way predicts, requiring only a single modification of the input BLF whenever it was changed by the spacecraft team (once every few months).

To support the Doppler tuner and TP-13/TP-2, the frequency predicts output from PG13 were run through additional routines that transformed the time frequency pairs into a series of Chebychev polynomials using an algorithm obtained from [10]. In addition, a software fix was implemented at the station to allow the metering of pointing predicts to the station’s antenna-pointing computer using Visual Basic for passes conducted up to the summer of 1998. After the station upgrade in the summer of 1998, a new interface consistent with the operational DSN was in place that allowed the direct import of a multiple predict point file. The format of the PG13 output pointing-angle file was modified to accommodate the new interface.

The delivery of predicts from JPL to DSS 13’s monitor and control (M&C) computer was nearly instantaneous over the NASA network connection to Goldstone using the file transfer protocol (FTP). At the station, the various predict sets were further processed and downloaded by station personnel to the destination subsystems. The PG13 frequency predict files were further processed for input to the ETT using special script files and templates that contained the desired tracking parameters, such as loop bandwidths and modes (aided or non-aided).

**Table 1. Ka-band downlink frequency modes.**

Ka-band frequency relation to X-band frequency (see text)	Mode description
$f_{ka(uso)} = 3.8f_{x(uso)}$	Pure one-way Ka-band
$f_{ka(vco)} = 3.8f_{x(vco)}$	Pure three-way Ka-band
$f_{ka(v/u)} = 4f_{x(vco)} - 0.2f_{x(uso)}$	Hybrid mode when X-band on VCO and S4 switch on USO
$f_{ka(u/v)} = 4f_{x(uso)} - 0.2f_{x(vco)}$	Hybrid mode when X-band on USO and S4 switch on VCO

## B. Station Operations

During each track, the station operations were governed by a sequence-of-events (SOE) file that was sent either by e-mail, FAX, or FTP to the station. This file listed station and spacecraft configurations as well as key events for the track. A typical track consisted of configuring the station for KaBLE-II; downloading predict information to the appropriate subsystem; performing precalibrations; acquiring the signal; peaking the antenna onto the signal (boresighting) (enabling monopulse tracking or manually determining pointing offsets); and reacquiring the signal (after periods of signal mode changes or occultation). After the track, data files were transferred into the appropriate subdirectory on the station computer, where they could be accessed by the data processor via FTP.

Once the receivers were locked onto the signals and the antenna properly pointed, station operations did not require significant operator intervention, except when unexpected problems or mode changes occurred. Diligent attention was required to make sure the data were being acquired properly. Problems that required prompt attention included occasional computer failures that necessitated reboots. Operations were less complicated during cruise, when received signal data usually were interrupted only during brief periods between mode changes. During orbit operations after 97-255, station operations were complicated by project activities such as moving the HGA off-Earth point or turning the spacecraft transmitter off during certain sequences, occultations (the spacecraft going behind the planet), and uncertain HGA pointing just after aerobraking events.

## V. Results

KaBLE-II data acquisition and analysis activities started on December 6, 1996, 1 month after launch and 1 month ahead of schedule. On that date, the Earth was 33 deg off the HGA boresight and drifting through the 130th Ka-band side lobe of the HGA, where pointing loss was  $-53 \pm 5$  dB. However, the MGS Ka-band signal was easily detected when tracked by the ETT in the aided mode. The received signal strength was 4.8 dB-Hz, as expected (see Fig. 10).

The next opportunity occurred on January 2, 1997, as Earth drifted through the boresight of the HGA. This signal was the strongest Ka-band signal ever to be received from MGS; the telemetry and ranging modulations were turned off, and the spacecraft never would be closer. January 17, 1997, was the first pass after the HGA was fixed on Earth point and radiated X-band and Ka-band. Figure 11 displays the residual carrier signals as tracked by the ETT for the January 2, 1997, pass (97-002).

Between January 1997 and December 1998, the Ka-band signal from MGS was tracked on a weekly basis along with the X-band signal, except during certain periods as detailed in Table 2. The two most common spacecraft operating modes while receiving Ka-band data were (1) the 60-deg telemetry modulation index used during the early stage of the mission (1997) and during solar corona in May 1998

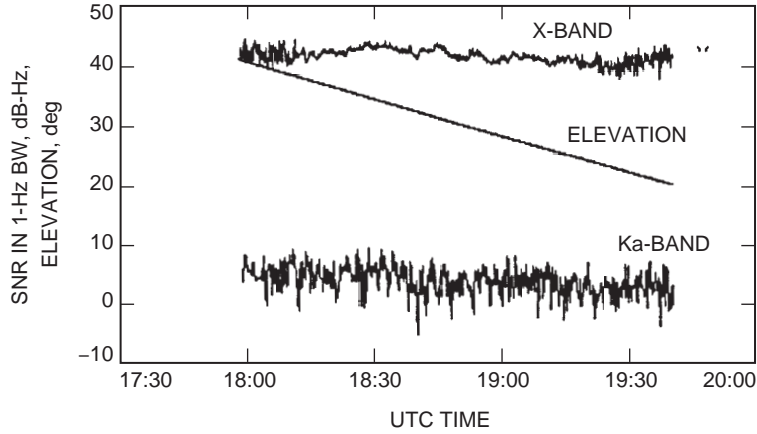


Fig. 10. 96-340  $P_c/N_o$  (X-band and Ka-band) and elevation angle.

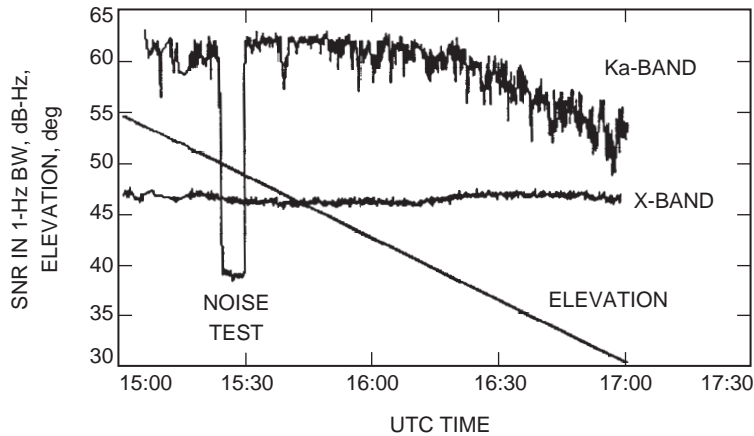


Fig. 11. 97-002  $P_c/N_o$  (X-band and Ka-band) and elevation angle.

when the spacecraft was using a low 21.333-kHz subcarrier frequency and (2) the 80-deg modulation index used during the high-rate data periods in 1997–1998 when MGS was transmitting high-rate science and engineering telemetry data on the higher 320-kHz subcarrier frequency. A few passes were conducted in which the data were acquired with an unmodulated carrier when the ranging and telemetry modulation were turned off (0-deg modulation index).

**Table 2. MGS mission and DSS-13 ground-station events for MGS/KaBLE-II.**

Calendar day	Year-day	Event
November 7, 1996	96-312	Launch.
December 6, 1996	96-341	Ka-band signal first detected and tracked (first light).
January 2, 1997	97-002	Earth passed through HGA boresight as the Ka-band signal was tracked with the strongest received signal strength.
February 4, 1997	97-035	Monopulse feed–receiver replaces array feed feed–receiver.
May 8, 1997	97-128	MGS went into emergency mode after performing maneuvers. HGA was 40-deg off Earth point during safing.
May 25, 1997	97-145	Safe mode exit.
June 4, 1997	97-155	Ka-band turned on.
August 6, 1997	97-218	Ka-band feed horn Rexalyte window replaced by fused-quartz window.
September 12, 1997	97-255	Mars orbit insertion (elliptical capture orbit).
September 27, 1997	97-270	Ka-band turned off.
October 4, 1997	97-277	Ka-band turned on.
October 12, 1997	97-285	Aerobraking suspended.
November 7, 1997	97-311	Aerobraking reinitialized.
January 23, 1998	98-023	KaBLE-II turned off on spacecraft (start of eclipses).
March 18, 1998	98-077	KaBLE-II turned back on.
April 30, 1998	98-120	Beginning of solar conjunction sequence, a cycle of 6 h Sun pointed and 2 h Earth pointed on HGA.
May 26, 1998	98-146	End of Solar corona period.
December 4, 1998	98-338	Ka-band core package replaces monopulse Ka-band package.
December 28, 1998	98-362	Ka-band turned off.

The following subsections describe results on X-band and Ka-band signal-strength data acquired during cruise and Mars orbit from December 1996 to December 1998, signal strength data acquired during MGS solar conjunction in May 1998, and dual-band frequency data acquired from January 1997 to May 1998, the telemetry demonstration, and the range demonstration.

### A. Signal-Strength Data

Table 3 is the experiment log that lists all of the tracking passes during which DSS 13 was scheduled to track MGS and which were not canceled due to unforeseen conflicts with other experiments. Listed in Table 3 are the experiment ID, the tracking mode (one-way or three-way), the modulation index in degrees, and the measured  $P_c/N_o$  signal strength at Ka-band for that pass if sufficient data were acquired and the ground antenna was believed to be on point.

A total of 197 tracking passes were conducted between December 1996 and December 1998 (see Table 3 for a listing). In the majority of the passes (181), a Ka-band signal was detected, locked onto, and tracked for a significant duration of each track. For 16 passes, Ka-band signals were not detected due to excessive solar corona noise angularly near the Sun (8 passes), ground-station equipment failures (6 passes), excessive spacecraft HGA mispointing during the entire track (1 pass), or short notice changes initiated by the MGS Project that impacted DSS-13 data acquisition (1 pass).

**Table 3. MGS/KaBLE-II experiment log.**

Experiment (year-day of year)	Mode	Telemetry modulation index, deg	Ka-band $P_c/N_o$ , dB-Hz	Notes and comments
S4 → USO				
96-341	1-way	—	7.2	(3) HGA off Earth point 30 deg. X-band on LGA.
97-002	1-way	00	62.2	(3) Earth passes through HGA boresight. X-band on LGA.
97-017	1-way	80	53.9	Clear. (3)
S4 → VCO				
97-022	3-way	60	48.8	(3)
S4 → USO				
97-023	1-way	60	47.1	Cloudy. (1) (3)
97-024	1-way	60	46.6	Partly cloudy. (1) (3)
	3-way	60	51.2	(2) (3)
97-027	3-way	60	50.0	Clear. (2) (3)
97-028	1-way	60	47.2	Partly cloudy. (1) (3)
S4 → VCO				
97-035 Monopulse receiver installed. Array feed removed.				
97-037	3-way	80	48.6	Initial monopulse test pass.
97-038	1-way	80	—	(4) Monopulse test pass.
97-041	3-way	80	47.8	(2) Antenna pointing failure.
97-042	3-way	80	47.7	(2)
97-044	1-way	60	44.9	Glitches in Ka-band data.
97-045	3-way	60	48.9	Clear. (2) Antenna pointing failure.
97-048	3-way	60	50.5	Cloudy. (2)
97-051	3-way	80	—	Windy. (2) Array feed/monopulse test. TPR BW(X) = 10 MHz.
97-052	3-way	80	—	Clear. (2) Array feed/monopulse test.
	1-way	80	—	—
97-062	3-way	60	48.3	Clear and windy. Data noisy past 12:30 UTC.
97-063	3-way	60	48.3	Clear. (2)
97-064	1-way	60	40.3	Ka-band signal-level reduction at 12:56:22–12:57:53 UTC.
	3-way	60	48.1	(2)
97-065	3-way	60	48.0	(2) Signal-level variations.
	1-way	60	—	—

(1) Accordion-like signature; warm-up transient and variation.

(2) Periodic 3-dB ranging spikes.

(3) Ka-band used the array feed package.

(4) Unable to maintain ground-station pointing (insufficient or no monopulse tracking; no offsets applied).

**Table 3 (contd)**

Experiment (year-day of year)	Mode	Telemetry modulation index, deg	Ka-band $P_c/N_o$ , dB-Hz	Notes and comments
S4 → USO				
97-070	3-way	60	46.5	Several level variations.
97-071	1-way	60	—	(1) (4)
97-072	1-way	60	43.6	(1)
97-073	1-way	60	42.7	(1)
97-077	3-way	60	47.4	Variations.
S4 → VCO				
97-078	3-way	60	46.2	Clear. Warm up transient. Diminished peak-to-peak variations.
97-079	3-way	60	46.1	Calm/clear. Variations, 3 dB at 6:50 UTC.
97-080	3-way	60	46.8	Clear. Variations, very small.
S4 → USO				
97-084	1-way	60	40.5	Ka-band data acquired near end of pass. Antenna went to brake. Restarted at 06:45 UTC.
97-085	1-way	60	40.4	Clear. Noisy data.
97-088	1-way	60	—	(4) Clear. Short period of degraded Ka-band near end of pass.
S4 → VCO				
97-091	1-way	60		(4) Clear. Variations on Ka-band.
S4 → USO				
97-092	1-way	00	53.4	Clear. Modulation turned off. Monopulse testing activities.
S4 → VCO				
	3-way	60	—	—
97-094	3-way	80	42.4	Variations at start removed.
97-098	3-way	80	39.4	Noisy periods.
	1-way	80	41.6	—
97-099	3-way	80	42.0	Few spurious glitches.
	1-way	80	41.4	—

(1) Accordion-like signature; warm-up transient and variation.

(2) Periodic 3-dB ranging spikes.

(3) Ka-band used the array feed package.

(4) Unable to maintain ground-station pointing (insufficient or no monopulse tracking; no offsets applied).

**Table 3 (contd)**

Experiment (year-day of year)	Mode	Telemetry modulation index, deg	Ka-band $P_c/N_o$ , dB-Hz	Notes and comments
97-100	3-way	80	42.4	—
97-105	3-way	60	—	(4) Clear. Insufficient data.
	1-way	60	—	Some variations at start of pass.
97-106	3-way	60	43.2	Clear. (1) 7-dB jump at 5:12 UTC.
97-107	3-way	60	43.9	Clear. (1) Short drop out at 4:36 UTC.
97-108	3-way	60	43.7	Clear. (1)
97-112	3-way	60	42.9	Clear. (1)
97-113	3-way	60	—	(4) Clear. Variations. Monopulse in monitor mode. Signal drop at 5:10 UTC.
	3-way	80	—	—
97-114	3-way	60	—	(4) Small variations “turn-on” transient. AMC gate way locked up 06:10; reloaded. High winds.
97-115	1-way	60	36.4	Clear. Small variations.
	3-way	60	42.1	Signal-level drop at 6:35–6:39 UTC.
97-119	3-way	60	—	(4) Significant signal degradation.
	1-way	60	—	—
97-120	3-way	60	41.7	Cloudy. (1)
97-121	3-way	60	40.6	Cloudy. Transient, small variations. Noisy.
97-122	3-way	60	41.7	Clear. (1)
97-123	3-way	60	41.3	Clear. (1) Smaller peak-to-peak accordion signature.
97-126	3-way	60	—	(4) Partly cloudy. Small variations.
97-127	1-way	60	34.7	Partly cloudy/clear.
97-129 Spacecraft went into safe mode. (Spacecraft emergency.) S4 → VCO				
97-155 Reacquiring Ka-band data. Ka-band turned back on. Start of feed horn ice accumulation period.				
97-155	3-way	60	—	Cloudy.
97-160	3-way	60	—	Clear. Data degraded. X-band $-4.2$ dB below predict.
	1-way	60	—	Data degraded. X-band $-4.3$ dB below predict.
97-162	3-way	60	—	Clear. Some wind. X-band degraded. Large signal-level drop at 3:35 UTC.
	1-way	60	—	—
97-167	1-way	60	—	Antenna-pointing failure from 20:40–21:20. Ka-band degraded.
97-169	1-way	60	—	Clear. Data degraded.
	3-way	60	—	Data degraded.
97-174	1-way	60	—	Clear. Data degraded.
	3-way	60	—	Data degraded.

(1) Accordion-like signature; warm-up transient and variation.  
(2) Periodic 3-dB ranging spikes.  
(3) Ka-band used the array feed package.  
(4) Unable to maintain ground-station pointing (insufficient or no monopulse tracking; no offsets applied).

**Table 3 (contd)**

Experiment (year-day of year)	Mode	Telemetry modulation index, deg	Ka-band $P_c/N_o$ , dB-Hz	Notes and comments
97-176	1-way	60	—	Clear. Data degraded.
	3-way	60	—	Data degraded.
97-182	1-way	80	—	Clear. Significant Ka-band degradation.
	3-way	80	—	Data degraded.
97-183a	1-way	80	—	Clear. Data degraded.
97-183b	3-way	60	—	Data degraded.
	1-way	60/80	—	—
97-188	1-way	80	—	Clear. Noisy. Ka-band very weak at 8 dB-Hz.
	3-way	80	—	Data degraded.
97-190	3-way	60	—	Clear. Data degraded.
97-195	1-way	60	—	Data degraded.
	3-way	60	—	Data degraded.
97-198	1-way	0	—	Cloudy. Data degraded.
97-202	3-way	60	—	100% clouds. Data degraded.
97-203	3-way	60	—	Rainy/clouds. Data degraded. Significant Ka-band variations at start of pass.
97-205	3-way	60	—	Clear. Data degraded.
97-206	—	—	—	X-band uplink failed to get into spacecraft (DSN Discrepancy Report A01517)
Ice fix 97-206. Warm up/cool down. 97-218 Feed horn window replaced.				
97-209	3-way	60	33.4	Thunder clouds at start of pass.
97-210	3-way	60	33.5	Clear/calm.
97-212	3-way	60	33.4	Partly cloudy.
97-217	3-way	80	33.1	Variations with 1-h 40-min period. TPR glitch at 01:59:26 UTC.
97-218	3-way	80	33.5	Scattered clouds. 1-h 40-min variations. TPR glitches at 23:16:59, 01:11:50, 03:29:14.
97-224	3-way	80	33.5	Clear and partly cloudy. Variations.
97-226	3-way	80	34.3	Clear. Variations.
97-230	3-way	80	33.5	Cloudy. Variations at spacecraft rotation period.
97-232	3-way	60	32.2	Clear.
	3-way	80	32.6	—
97-237	3-way	80	32.9	Partly cloudy. Periodic.
97-239	3-way	80	33.2	Clear. Variations.
97-280	3-way	80	—	Insufficient TPR data.
97-282	3-way	80	30.2	Light clouds.
<p>(1) Accordion-like signature; warm-up transient and variation.</p> <p>(2) Periodic 3-dB ranging spikes.</p> <p>(3) Ka-band used the array feed package.</p> <p>(4) Unable to maintain ground-station pointing (insufficient or no monopulse tracking; no offsets applied).</p>				

**Table 3 (contd)**

Experiment (year-day of year)	Mode	Telemetry modulation index, deg	Ka-band $P_c/N_o$ , dB-Hz	Notes and comments
97-294	3-way	80	32.0	—
97-295	3-way	80	29.5	Clear. Small variations.
97-297	3-way	80	30.5	(4) Clear/windy. Variations.
97-300	3-way	80	28.3	Light to moderate clouds. Very short period of Ka-band data.
97-301	3-way	80	30.5	Clear.
97-302	3-way	80	30.4	Clear/high light clouds.
97-307	3-way	80	—	Light to medium high scattered clouds. No ETT data.
97-308	3-way	80	29.9	—
97-309	3-way	80	—	(4) Clear.
97-314	3-way	80	27.0	Heavy clouds. Variations, glitches.
97-315	3-way	80	29.1	X-band variations between 23–24 UTC.
97-316	3-way	80	27.9	Cloudy. Project spacecraft activities between 23:00–24:00 UTC.
97-325	3-way	80	26.4	—
97-337	3-way	80	28.1	Clear. 2-dB variations with 1-h 40-min period.
97-344	3-way	80	26.9	Clear/cold. Noisy 00:15–02:20. Periodic drop outs.
97-351	3-way	80	29.7	—
97-364	3-way	80	30.1	Clear. Large negative downward drift in signal level.
97-365	3-way	80	26.0	Partly cloudy. No plots.
98-005	3-way	80	25.9	Clear. Small variations 1 h 40 in.
98-006	3-way	80	25.8	Partly cloudy/high cirrus. Antenna computer failure. Small variations 1-h 40-min period.
98-008	3-way	80	25.0	Clear and calm. 1-h 40-min variations. Dual Ka-band pass.
98-009	3-way	80	26.0	Cloudy. Variations.
98-013a	3-way	80	—	Poor. Radiometer/pointing problems. TPR Ka-band $T_{op}$ invalid 28–35 K. TPR glitches.
98-013b	3-way	80	28.6	Clear. Ranging off command exercised at 00:12:43 UTC.
98-014	3-way	80	—	Clear. Ranging off command exercised. 1-h 40-min variations. TPR data incorrect format.
98-016	3-way	80	—	No ETT X-band data acquired.
98-019	—	—	—	DSS-13 equipment failure. Pass never conducted.
S4 → USO at 98-020/20:23:24				
98-020	3-way	80	28.5	Cloudy.
S4 → VCO at 98-021/01:23:21				
98-021	3-way	80	—	Clear. Dual Ka-band pass. No X-band data.

(1) Accordion-like signature; warm-up transient and variation.  
(2) Periodic 3-dB ranging spikes.  
(3) Ka-band used the array feed package.  
(4) Unable to maintain ground-station pointing (insufficient or no monopulse tracking; no offsets applied).

**Table 3 (contd)**

Experiment (year-day of year)	Mode	Telemetry modulation index, deg	Ka-band $P_c/N_o$ , dB-Hz	Notes and comments
98-023/20:30 Ka-band turned off S4 → USO 98-077/18:00 Ka-band turned back on				
98-080	3-way	80	—	Dual Ka-band pass with DSS-14 array feed. No ETT X-band data.
98-082	3-way	80	30.0	Unknown 3- to 4-dB signal-level drop around 23:43 UTC.
98-083	3-way	80	26.6	Clear. Dual Ka-band DSS 14/DSS 13 for part of pass.
98-084	1-way	80	—	Cloudy/rain. Ka-band data degraded.
	3-way	80	24.5	Variations. Noisy. Glitches.
98-086	3-way	80	—	ETT failure.
	1-way	80	—	—
98-089	3-way	80	26.7	Clear.
	1-way	0	27.7	—
98-090	3-way	80	25.5	Huge rain cell between 00:30–01:00 UTC.
98-091	1-way	80	—	—
	3-way	80	25.8	—
98-093	1-way	80	—	Cloudy.
	3-way	80	27.9	Monopulse gain changed –10 dB. Recalibrated.
98-096	3-way	80	27.3	Clear. Computer failure 18:00 UTC. HGA off pointing.
	1-way	0	24.7	—
98-097	—	—	—	Power failure. No data.
98-100	1-way	0	19.7	Clear. Huge frequency ramp residuals.
	3-way	80	—	(4)
98-103	3-way	80	24.4	(4) Clouds come and go. Gusty winds. Noisy data. Glitches in TPR data.
	1-way	0	—	(4)
98-104	3-way	80	25.5	(4) Clear and windy.
	1-way	0	17.2	(4)
98-105	3-way	80	25.7	Windy, clouds. Monopulse gain changed +10 dB. Recalibrated. Antenna braked at 23:20.
	1-way	0	24.5	—
98-107	3-way	80	25.5	Clear.
98-113	3-way	80	—	Winds/clear. Clouds on horizon. Data noisy. Dual Ka-band DSS 14/DSS 13.
98-114	3-way	80	24.2	Sky clear with some occasional puffy clouds.

(1) Accordion-like signature; warm-up transient and variation.

(2) Periodic 3-dB ranging spikes.

(3) Ka-band used the array feed package.

(4) Unable to maintain ground-station pointing (insufficient or no monopulse tracking; no offsets applied).

**Table 3 (contd)**

Experiment (year-day of year)	Mode	Telemetry modulation index, deg	Ka-band $P_c/N_o$ , dB-Hz	Notes and comments
Solar corona period start S4 → USO				
98-118	3-way	60	—	Clear. No Ka-band data. Project changed BLF.
98-119	1-way	60	12.6	—
	3-way	—	—	No usable 3-way Ka-band data. Project changed BLF.
98-121a	3-way	60	27.1	Clear. Large frequency ramps. No MP. Predict loading problem. Sporadic lock periods.
	1-way	60	24.3	—
98-121b	3-way	60	27.7	—
	1-way	60	25.1	—
98-124a	3-way	60	23.0	Cloudy. Large frequency ramps.
	1-way	60	23.4	—
98-125a	3-way	60	19.5	Ka-band very noisy.
	1-way	60	17.4	—
98-125b	1-way	60	16.5	Operational DSN uplink failed.
98-126a	1-way	60	21.4	Overcast.
98-126b	1-way	60	21.4	HGA off Earth point.
98-128a	1-way	60	15.7	—
98-128b	1-way	60	—	—
98-129a	1-way	60	—	—
98-130a	1-way	60	—	Cloudy and windy.
98-130b	1-way	60	—	Clear and windy.
98-131a	1-way	60	—	Clear.
98-131b	1-way	60	—	Clear/windy.
98-132 Superior conjunction. MGS/Mars behind Sun.				
98-134a	1-way	60	—	Puffy white clouds in sky.
98-135a	1-way	60	—	Clear.
98-135b	1-way	60	19.8	Clear/good.
98-136a	1-way	60	21.5	Light clouds. TPR problems.
98-136b	1-way	60	—	Clear, some high clouds. TPR problems.
98-138a	3-way	60	21.9	Clear.
	1-way	60	23.3	—
98-139a	3-way	60	—	Clear. HGA off Earth point, 10 deg.
98-139b	1-way	60	20.2	Light clouds. HGA off Earth point, >1 deg.
<p>(1) Accordion-like signature; warm-up transient and variation.</p> <p>(2) Periodic 3-dB ranging spikes.</p> <p>(3) Ka-band used the array feed package.</p> <p>(4) Unable to maintain ground-station pointing (insufficient or no monopulse tracking; no offsets applied).</p>				

**Table 3 (contd)**

Experiment (year-day of year)	Mode	Telemetry modulation index, deg	Ka-band $P_c/N_o$ , dB-Hz	Notes and comments
98-140a	1-way	60	18.6	Clear. HGA off Earth point.
	3-way	60	—	—
98-140b	1-way	60	21.4	Partly cloudy. HGA off Earth point.
98-141a	3-way	60	25.8	Clear.
	1-way	60	23.1	—
98-142a	3-way	60	26.1	Clear. HGA off Earth point. TPR problems.
	1-way	60	23.4	—
98-146a	—	—	—	Clear.
Solar corona period end S4 → VCO DSS-13 station upgrade July 1998; new computer interface installed				
98-161a	3-way	80	26.4	Cloudy. Dual Ka-band acquired during part of pass.
98-162a	3-way	80	26.2	Clear. Dual Ka-band acquired during part of pass. Antenna failure.
98-181a	3-way	80	—	Clear. X-band system failure. No X-band calibration data.
98-187a	3-way	80	—	Clear. TPR/noise diode failure. HGA 0.9-deg off point. No X-band calibration.
98-189a	3-way	80	—	Partly cloudy. HGA off Earth point. Ka-band $T_{op} = 207$ K. Compressor failure.
98-203a	1-way	80	—	HGA off Earth point. Predict mode failure. Used planetary mode to point.
S4 → USO at 98-203/15:00 S4 → VCO at 98-204/14:00				
98-208a	3-way	80	—	Clear and hot. SSPA temperature <30 deg C. Ka-band data noisy.
98-210a	1-way	80	—	Clear and hot. SSPA variations. Ka-band data noisy.
	3-way	80	25.2	00:28:13, 03:01:29 TPR glitches. Minicalibrations performed during pass.
98-215a	3-way	80	—	(4) Clear. TPR X- and Ka-band anticorrelated data noisy.
98-217a	3-way	80	—	TPR file lost. No X-band data.
98-222a	3-way	80	—	Cloudy. No X-band.
98-224a	1-way	80	—	Incorrect pointing model loaded. SSPA 30.3 deg C. Manual offsets used. Only 2-min Ka-band data.
98-229a	3-way	80	26.5	Manual offsets used. 21:30–22:30 TPR noisy. Used last segment only.
	1-way	80	—	—
<p>(1) Accordion-like signature; warm-up transient and variation.</p> <p>(2) Periodic 3-dB ranging spikes.</p> <p>(3) Ka-band used the array feed package.</p> <p>(4) Unable to maintain ground-station pointing (insufficient or no monopulse tracking; no offsets applied).</p>				

**Table 3 (contd)**

Experiment (year-day of year)	Mode	Telemetry modulation index, deg	Ka-band $P_c/N_o$ , dB-Hz	Notes and comments
98-231a	3-way	80	—	X-band radio frequency interference. No TPR data. IF switch failure. MP error channel lost power. Station released.
98-236a	1-way	80	—	X-band TPR data erroneous.
	3-way	80	26.1	—
98-243a	1-way	80	—	Crystal frequency values revised in monopulse code.
	3-way	80	26.0	Lost TPR data.
98-245a	1-way	80	—	—
	3-way	80	25.5	Partly cloudy. SSPA 29.97 deg C.
98-251	3-way	80	25.5	Scattered clouds. Antenna computer problem.
98-252a	3-way	80	—	Partly cloudy. Project operating with 8.4-kHz FRO. X-band on auxiliary oscillator.
98-258a	3-way	80	25.4	Clear. TPR filters reversed. Monopulse predict set load problem. HGA mispointing.
98-259a	1-way	80	—	Partly cloudy.
	3-way	80	25.4	Degraded data 19:00–19:38. X-band TPR not calibrated.
98-265/20:00 KaBLE-II turned back on $T = 22.5$ deg C S4 → USO				
98-266a	3-way	80	27.6	Clear, light winds. TPR data only from 19:34 to 20:38 UTC. ETT network problems. Ka-band power meter not calibrated.
	1-way	80	—	—
98-272a	3-way	80	26.2	Clear. Significant frequency drifts. Monopulse calibration problems; MP cable misconfigured at start.
98-273a	3-way	80	26.4	—
S4 → VCO at 98-274/00:48				
98-279a	3-way	80	24.9	No MP data.
98-280a	3-way	80	24.2	Clear. Winds calm. Track mode at 17:19. Autobores performed.
98-300a	3-way	80	23.8	Clear. No monopulse pointing control. Applied manual offsets.
98-301a	3-way	80	23.2	Clear. No Monopulse pointing control. Used manual offsets.
98-306a	3-way	80	—	80% cloudy. No monopulse interface to antenna.
98-313a	3-way	80	20.0	95% clear. Missing TPR data for 19:41–21:22. Manual offsets applied. Monopulse started tracking at 20:45 UTC.
98-314a	3-way	80	18.3	Clear. Light scattered clouds. Antenna interface down. Used manual offsets. Ka-band 7.5-kHz below predict.

(1) Accordion-like signature; warm-up transient and variation.

(2) Periodic 3-dB ranging spikes.

(3) Ka-band used the array feed package.

(4) Unable to maintain ground-station pointing (insufficient or no monopulse tracking; no offsets applied).

**Table 3 (contd)**

Experiment (year-day of year)	Mode	Telemetry modulation index, deg	Ka-band $P_c/N_o$ , dB-Hz	Notes and comments
98-320a	3-way	80	12.9	Clear. Unscheduled aerobraking maneuver burn. Unable to lock monopulse. No TPR data.
98-328a	3-way	80	21.2	Clear.
98-329a	3-way	80	18.7	Clear. Monopulse started tracking at 18:46 UTC.
98-335a	3-way	80	19.8	—
98-342a	3-way	80	12.0	Clear. No monopulse pointing control.
98-357a	3-way	80	—	Clear. No Ka-band signal.

(1) Accordion-like signature; warm-up transient and variation.  
(2) Periodic 3-dB ranging spikes.  
(3) Ka-band used the array feed package.  
(4) Unable to maintain ground-station pointing (insufficient or no monopulse tracking; no offsets applied).

For 181 passes, a Ka-band signal was locked onto and tracked for a significant duration of the pass. The received signal strengths vary due to spacecraft range, mispointing, modulation index, ranging modulation, ground-station configuration, weather attenuation, KaBLE-II flight temperature, and downlink frequency. Eighteen of these passes (from 97-155 to 97-206) were considered unusable due to a crack in the feed horn window that caused ice to accumulate inside the horn. An additional 31 passes were not used due to insufficient ground-antenna pointing control and failure to acquire calibration ( $T_{op}$ ) data.

For 132 passes, the Ka-band signals were tracked with minimum ground-station pointing loss using monopulse pointing control (or array feed compensation during December 1996 through January 1997) or manual pointing-angle offsets. The average atmospheric attenuation for these passes varied from 0.1 to 0.9 dB.

Most data were acquired by tracking the residual carrier with the ETT and the spacecraft configured on the HGA. Telemetry and ranging modulation suppressed the residual carrier by varying amounts, depending on the modulation index. In order to estimate the total signal power and the EIRP for comparison purposes, the measured carrier was “corrected” for these suppression effects. These corrected values of EIRP generally were not in agreement for Ka-band. This was expected due to known anomalies in the KaBLE-II flight hardware (modulation index uncertainty, spurs at different frequencies, and operating temperatures). However, when telemetry and ranging were turned off and all of the power was in the carrier, as on April 2, 1997 (97-092), the observed Ka-band SNR agreed with prediction to within 1 dB. Figure 12 illustrates this during a period of a few minutes duration. When correcting for spacecraft equipment deficiencies at Ka-band, the result confirms the expected 5- to 6-dB Ka-band link advantage over X-band and confirms that antenna pointing loss has been minimized.

The EIRP was inferred as follows: The received carrier power was estimated from the ETT  $P_c/N_o$  signal/noise and the TPR noise measurements. The received data then were corrected for ground-station gain [6], atmospheric attenuation, and space loss, producing estimates of the EIRP at the spacecraft. These EIRP estimates then were compared with the predicted “ideal” EIRP of 82 dBm at X-band and 76 dBm at Ka-band measured prior to launch.

Figure 13(a) is an example of X-band and Ka-band carrier ( $P_c/N_o$ ) data acquired during a clear-weather pass conducted on 97-212. Figure 13(b) displays the concurrent  $T_{op}$  data recorded at Ka-band for this pass. Figure 14(a) is an example of  $P_c/N_o$  data acquired during a cloudy and rainy weather pass on 97-203. Figure 14(b) displays the Ka-band  $T_{op}$  data recorded at Ka-band for pass 97-203. Note that the signal-level variations in the Ka-band  $P_c/N_o$  in Fig. 14(a) for the cloudy weather pass are clearly negatively correlated with the Ka-band  $T_{op}$  variations in Fig. 14(b).

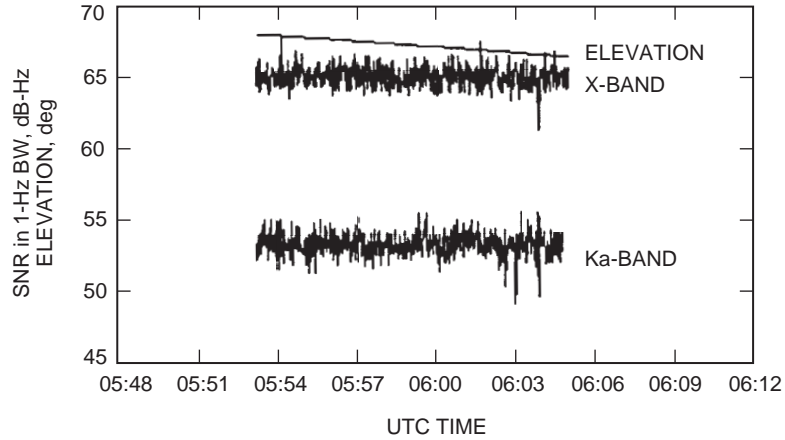


Fig. 12. 97-092  $P_c/N_o$  (X-band and Ka-band) and elevation angle.

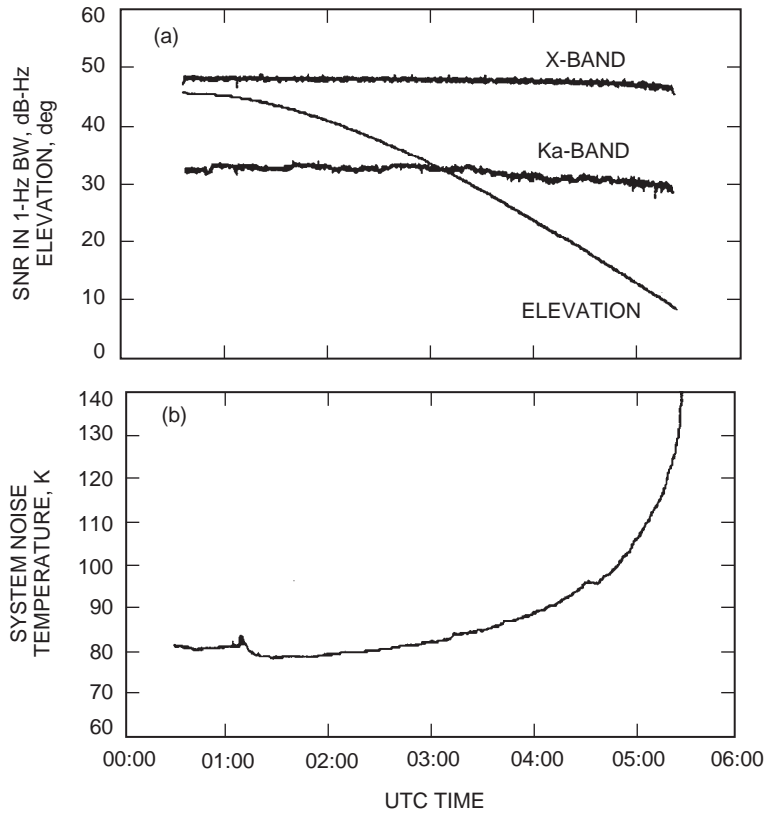


Fig. 13. 97-212 (a) X-band and Ka-band  $P_c/N_o$  and elevation angle and (b) Ka-band  $T_{op}$ .

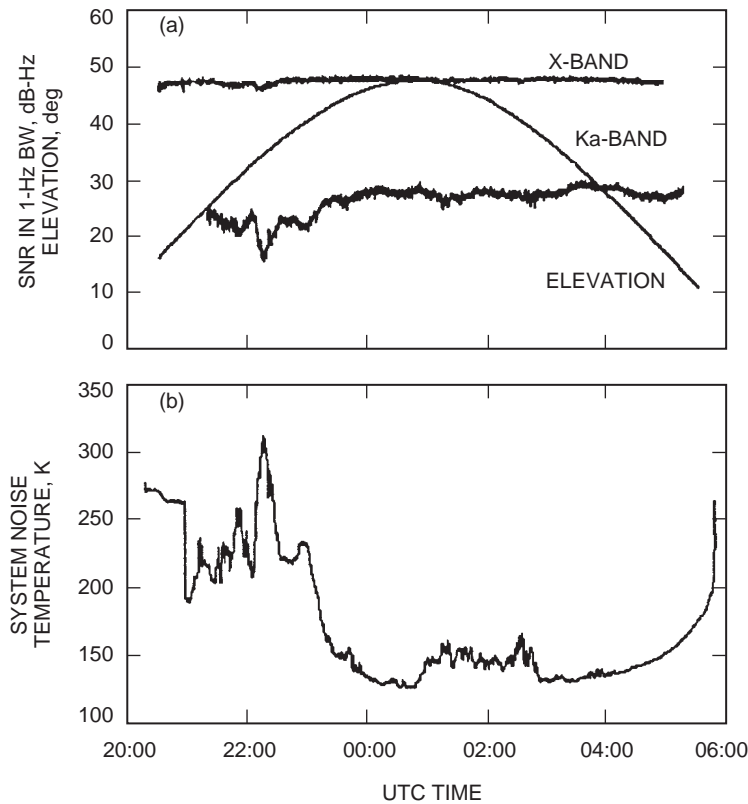


Fig. 14. 97-203 (a) X-band and Ka-band  $P_c/N_o$  and elevation angle and (b) Ka-band  $T_{op}$ .

Some passes produced  $P_c/N_o$  signatures that included anomalous problems. One anomaly encountered was the “accordion” effect in the received  $P_c/N_o$  data illustrated in Fig. 15(a), which is attributed to a transient response when the Ka-band equipment was turned on just before each pass. Another anomaly includes 3-dB up spikes in the measured  $P_c/N_o$  data attributed to a short portion of the ranging period when the carrier ranging was not suppressed, as observed during some of the three-way passes [Fig. 15(b)]. Another anomaly observed during some passes was the sinusoidal variation in received  $P_c/N_o$  due to the spacecraft HGA axis rotating about the spacecraft spin axis, which was off Earth point, causing 1-h and 40-min periodic variations [Fig. 15(c)].

Figure 16(a) displays the measured X-band and Ka-band ETT carrier-to-noise signal levels ( $P_c/N_o$ ) for each pass while the spacecraft was using a 61.5-deg telemetry modulation index at X-band (63.6 deg at Ka-band) along with predicted values (solid lines). Figure 16(b) displays the measured X-band and Ka-band ETT carrier-to-noise signal levels ( $P_c/N_o$ ) for each pass while the spacecraft was using a 79.6-deg telemetry modulation index at X-band ( $\approx 4 \times 79.6$  deg at Ka-band) along with predicted values (solid lines). Three-way peak signal strength data points are denoted by “3,” and the one-way data points are denoted by “1” on these plots. Each X-band data point represents the averaged value of signal strength over each data set. Each Ka-band data point represents the peak 100-s averaged value of signal strength over each data set, which spans anywhere from a few minutes to several hours. For some of the tracks for which the Ka-band data displayed significant sinusoidal variations [see Fig. 15(c)], this strategy removed much of the pointing error incurred over most of the pass due to the spacecraft spin (when the HGA boresight axis was misaligned with the spacecraft spin axis). These variations in signal level of about 2 dB were expected given the  $\sim 0.1$ -deg pointing knowledge of the spacecraft HGA.<sup>4</sup>

<sup>4</sup> C. Chen, *Mars Global Surveyor Project Telecommunications System Operations Reference Handbook*, Version 2.1, 542-257 (internal document), Jet Propulsion Laboratory, Pasadena, California, September 1996.

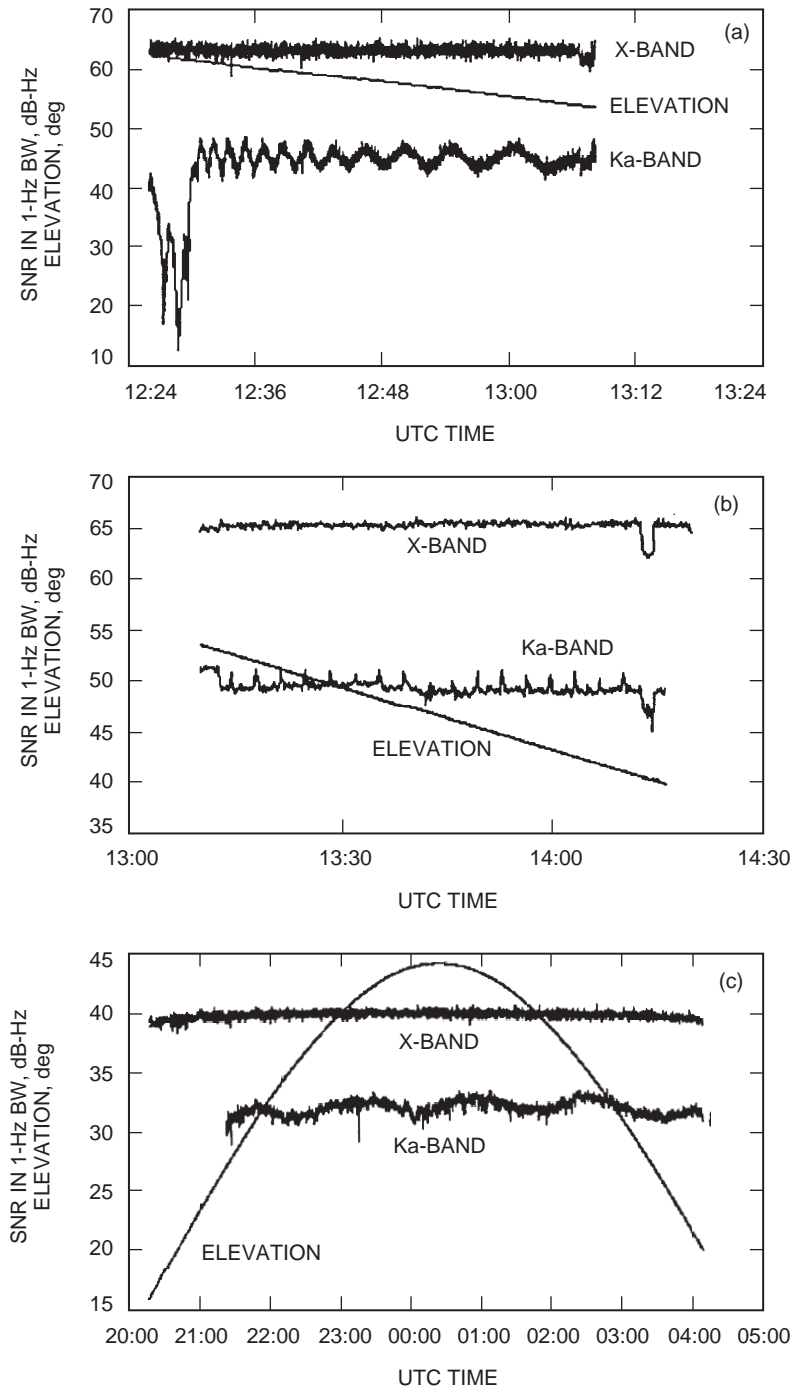
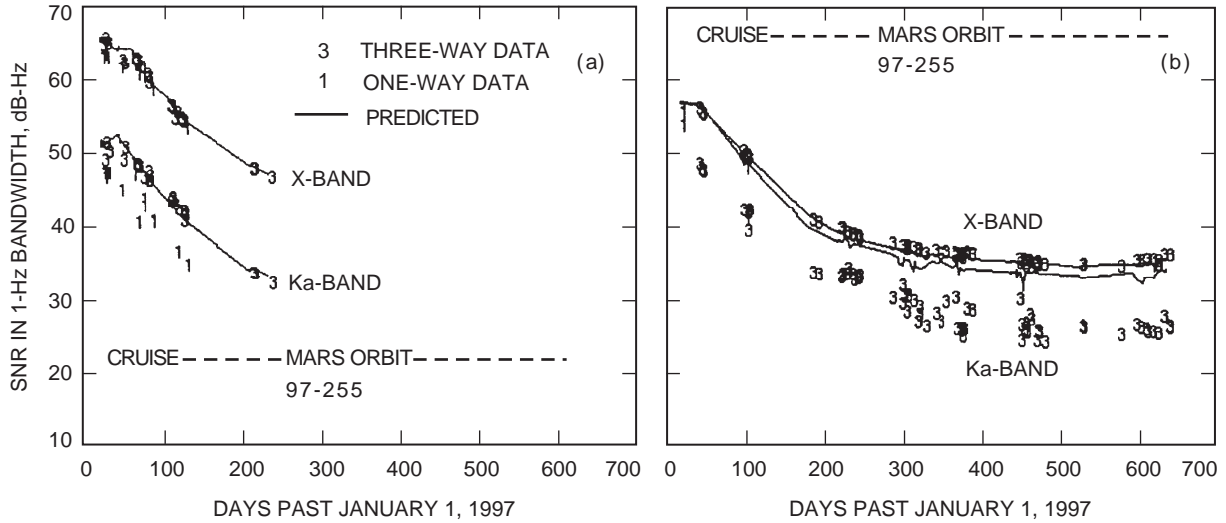


Fig. 15. Examples of (a) the accordion effect (97-024, one-way), (b) ranging 3-dB up spikes (97-024, three-way), and (c) spacecraft spin-induced variations due to HGA axis nonalignment (97-217).



**Fig. 16.  $P_c/N_o$  versus day of year for passes with a telemetry modulation index of (a) 61.5 deg at X-band and 63.6 deg at Ka-band (degraded data removed) and (b) 79.6 deg at X-band and  $79.6 \times 4$  deg at Ka-band.**

The predicted  $P_c/N_o$  values (solid lines in Fig. 16) have been derived based on the following parameters and assumptions: The spacecraft EIRP used is 82.4 dBm for X-band three-way data, 82.0 dBm for X-band one-way data (different due to measured HGA gain differences at different X-band frequencies), and 76.0 dBm for all Ka-band data.<sup>5</sup> No correction has been applied in the predicted values for any possible spacecraft mispointing. The space-loss correction used the range distances from the PG13 output files, which were computed from the navigation trajectory files input to PG13. The carrier-suppression correction due to ranging was 0.2 dB for X-band and 3.4 dB for Ka-band. The carrier suppression due to ranging was measured during test periods in experiments by taking the difference of the measured  $P_c/N_o$  before and after the ranging modulation was turned off or turned back on. The carrier-suppression correction due to telemetry modulation used modulation indices of 61.5 deg or 79.6 deg for X-band and 63.6 deg or  $4 \times 79.6$  deg for Ka-band. These modulation indices were estimated from carrier and data channel signal levels,  $P_c/N_o$  and  $P_d/N_o$ , acquired by DSS 13's advanced telemetry processor receivers (see Section III.C). The X-band value of 61.5 deg is consistent with an independent 61.2-deg value obtained from MGS X-band preflight measurements.<sup>6</sup> The 63.6-deg Ka-band modulation index is consistent within the 2.5-deg uncertainty of the X-band 61.5-deg modulation index when multiplied through the X4 multiplier. The thermal noise correction uses the  $T_{op}$  data obtained from the TPR (see Section III.D). The atmospheric-attenuation correction came from a model using input surface meteorological data. The ground-station gain correction uses antenna efficiencies measured from experiments using natural calibrator radio sources [6].

Table 4 summarizes the statistics of the residual (measured minus predicted)  $P_c/N_o$  signal levels for each of the spacecraft modes (three-way and one-way) and telemetry-modulation indices. Upon examination of the Table 4 statistics and Fig. 16, we find that the X-band  $P_c/N_o$  data are in agreement with the predicted values, ranging from 0 dB to  $-1.5$  dB depending upon the spacecraft mode and modulation index.

For the 63.6-deg telemetry-modulation index three-way case [see Fig. 16(a)], the Ka-band data appear to agree best with the predicted values. The observed minus predicted  $P_c/N_o$  residual of  $-0.7 \pm 0.8$  dB in Table 4 is the average value over all 27 passes for this case. These pass-to-pass statistics are consistent with 1- to 2-dB signal-level variations expected from the  $\sim 0.1$ -deg pointing knowledge of the spacecraft

<sup>5</sup> Ibid.

<sup>6</sup> W. Adams, personal communication, Lockheed-Martin Astronautics, February 9, 1998.

**Table 4. Residual (observed – predicted)  $P_c/N_o$ .**

Band	Mode	Telemetry modulation index, deg	Average $P_c/N_o$ residual, dB	Passes, no.	Total valid data, s
X	1-way	0	0.0	1	720
X	1-way	61.5	$-1.66 \pm 0.62$	16	105,831
X	3-way	61.5	$-1.03 \pm 0.62$	27	289,568
X	1-way	79.6	$-1.53 \pm 0.25$	3	18,252
X	3-way	79.6	$0.08 \pm 0.38$	65	846,529
Ka	1-way	0	-1.5	1	720
Ka	1-way	63.6	$-5.38 \pm 1.20$	11	59,865
Ka	3-way	63.6	$-0.74 \pm 0.84$	27	201,061
Ka	1-way	$79.6 \times 4$	$-6.07 \pm 2.61$	3	15,913
Ka	3-way	$79.6 \times 4$	$-6.92 \pm 1.62$	65	749,952

HGA. For the 63.6-deg telemetry-modulation index one-way case (see Fig. 16(a) and Table 4), the Ka-band signal-level data were biased 5 dB below that of the three-way data. This bias is believed to be attributed to a reduced response of the spacecraft equipment at the higher Ka-band one-way frequency (32.008 GHz) relative to the lower three-way frequency (31.986 GHz).

For the 79.6-deg modulation-index cases, the measured Ka-band signal levels lie 6 dB below the predicted values (see Fig. 16(b) and Table 4). These discrepancies are attributed to various effects of the flight hardware with the Ka-band signal due to (1) uncertainty in the carrier-suppression correction at the higher 318-deg modulation index at Ka-band (79.6 deg  $\times$  4) and (2) the effect of spurious energy at the higher 320-kHz subcarrier frequency<sup>7</sup> used at the 79.6 deg  $\times$  4 modulation index (the lower 21.333-kHz subcarrier frequency is used during the 63.6-deg modulation-index passes).

In addition to this bias, the scatter in the observed values increases significantly after Mars orbit insertion (September 12, 1997, or 97-255) due to larger HGA pointing errors occurring during this period, and because the SSPA temperature cycles below and above 30 deg C during an orbit period, where 30 deg C is the temperature threshold at which the equipment output signal level severely degrades (especially towards the end of the data acquisition). (See Figs. 17(a), 17(b), and 17(c) for examples of SSPA temperature.)

Figure 18(a) displays a projection (based on future ground and spacecraft performance trends) of the Ka-band link advantage (versus X-band) and error bars using the X-band and Ka-band data of Fig. 16 normalized to equal conditions. The data from passes conducted during the period of accumulated ice inside the feed horn (see Section III.A) and the solar corona experiment were not included in Fig. 18(b). This advantage is computed from the difference of the measured Ka-band and X-band  $P_c/N_o$  estimates that are corrected for preventable deficiencies at both bands. For equal spacecraft transmitted power, a 14-dB correction was applied (1 W at Ka-band versus 25 W at X-band). A 2.5-dB correction was applied to equalize for circuit losses, and a 1.6-dB correction was applied to equalize for spacecraft antenna efficiency. For expected future improved LNAs, the averaged  $T_{op}$  over each pass was adjusted accordingly (see the footnotes to Tables 5 and 6). The telemetry-modulation and ranging-channel carrier-suppression contributions were backed out for both X-band and Ka-band. An additional

<sup>7</sup> A. P. Mittkus, “KaBLE-II—System Discussions,” JPL Interoffice Memorandum 3363-97-020 (internal document), Jet Propulsion Laboratory, Pasadena, California, May 22, 1997.

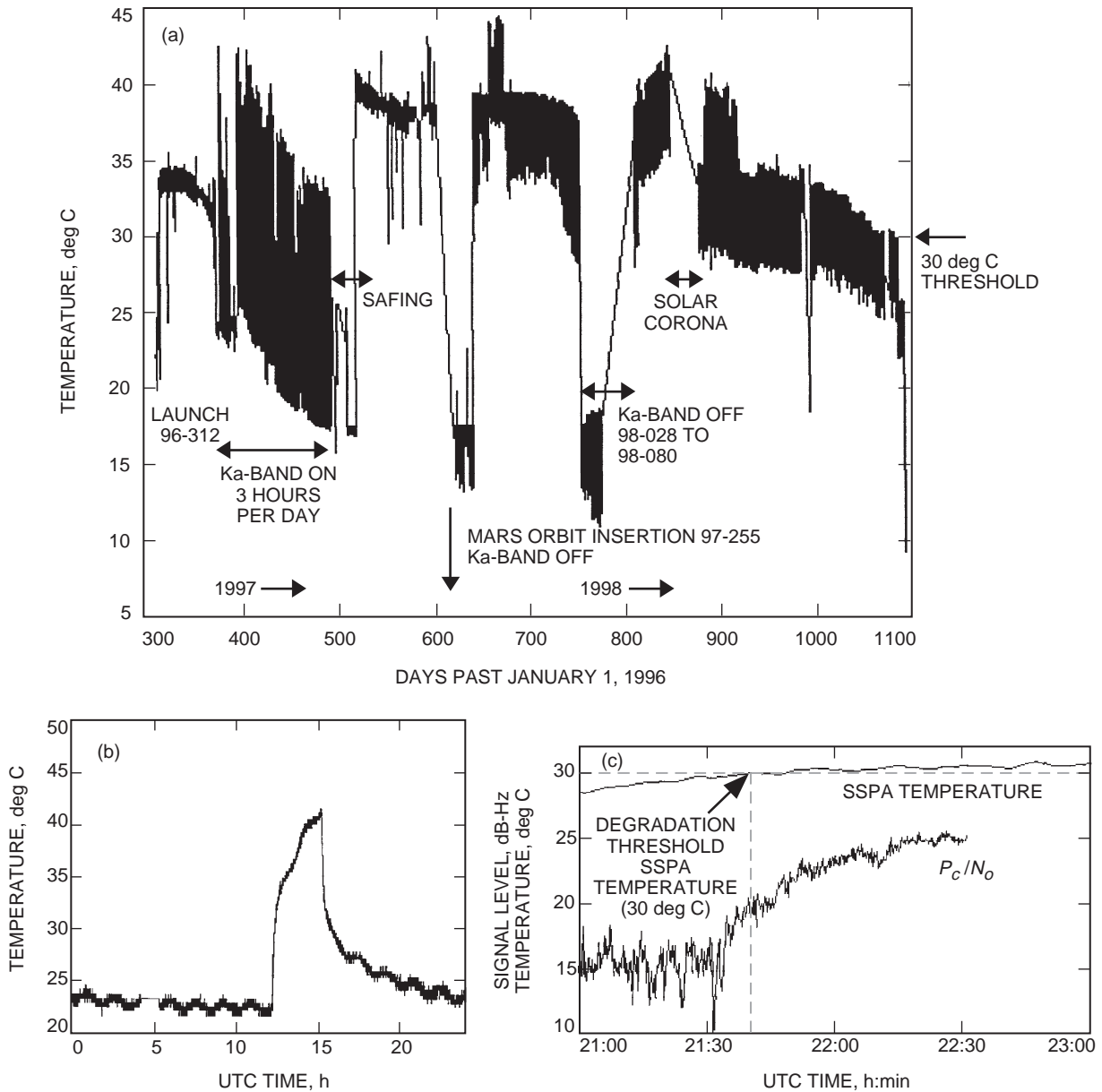


Fig. 17. MGS/KaBLE-II (a) Ka-band SSPA temperature versus days past January 1, 1996 (obtained from MGS telemetry), (b) SSPA temperature versus time of day for a single day, 97-027, and (c) Ka-band SSPA temperature and Ka-band  $P_c/N_o$  versus UTC for 98-210.

4.9-dB correction was applied to the one-way data based on the measured difference between three-way and one-way data segments within a common pass. A measured 5.7-dB correction was applied to Ka-band measurements acquired at the  $79.6 \times 4$ -deg modulation index. These corrections are illustrated for both the 60- and 80-deg cases in Tables 5 and 6, respectively, for pass 97-232. The result displayed in Fig. 18(b) confirms the predicted 5-dB Ka-band link advantage over X-band and, by implication, the minimized spacecraft antenna-pointing loss for these passes, which occurred during cruise before going into orbit around Mars. The lower advantage measured after going into Mars orbit is attributed to the degraded HGA pointing incurred at Ka-band during this phase of the mission and additional degradation due to the increased probability of the Ka-band SSPA temperature going below 30 deg C during an orbit cycle [see Fig. 17(a)], where the transmitted carrier-signal level is known to degrade.

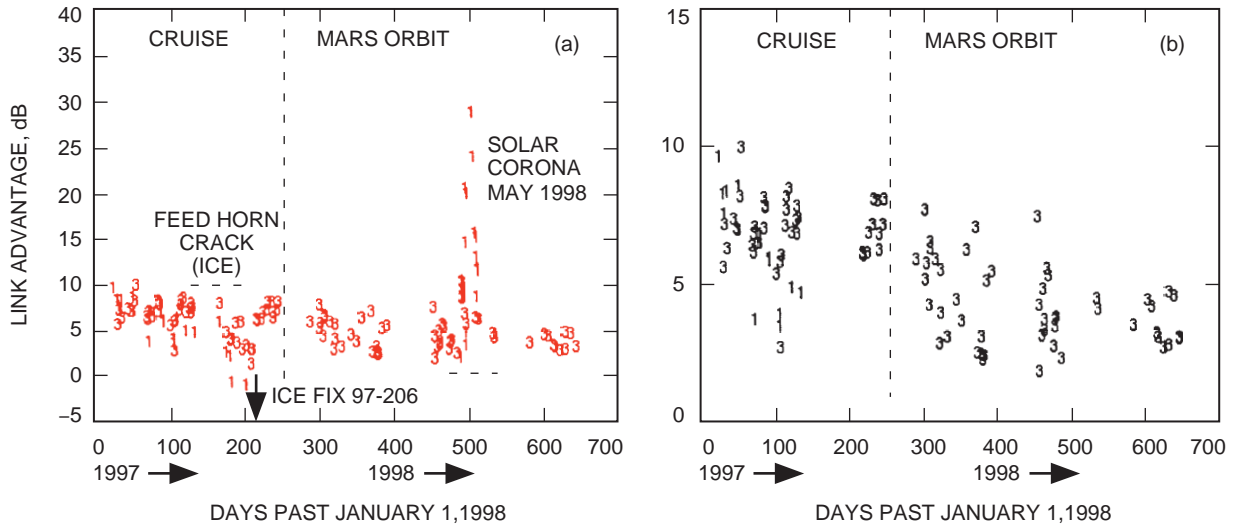


Fig. 18. Ka-band link advantage versus day of year for (a) all data and (b) all data except the solar corona and the cracked feed horn ice period.

Table 5. MGS/KaBLE-II link advantage, pass 97-232, 60-deg modulation index case.

Parameter	X-band	Ka-band	Delta, dB
Measured $P_c/N_0$	46.6 dB-Hz	32.2 dB-Hz	-14.4
Power	25 W	1.2 W	13.2
Antenna gain	39 dBi	49 dBi	1.6
Circuit loss	1.0 dB	3.5 dB	2.5
Net EIRP correction	—	—	17.3
Ranging suppression	0.2 dB	3.4 dB	3.2
Telemetry suppression	6.4 dB	7.0 dB	0.6
LNA temperature <sup>a</sup>	3.3 dB (49 K)	2.2 dB (82 K)	-1.1
Net advantage	—	—	5.6

<sup>a</sup>Note that the LNA correction for X-band is  $-10 \log[(T_{op} - 26)/T_{op}]$ , and for Ka-band it is  $-10 \log[(T_{op} - 33)/T_{op}]$ .

The Ka-band solid-state power amplifier (SSPA) temperature measurements obtained from spacecraft telemetry from launch (96-312) to the end of the data acquisition (98-364) are displayed in Fig. 17(a). For passes conducted during early 1997, the Ka-band equipment was turned on for only 3 hours a day. The wide temperature range during this period depicted in Fig. 17(a) is displayed more clearly for a single daily cycle in Fig. 17(b). During the signal-strength data acquisition, there usually is a warm-up transient observed at the beginning [see the example in Fig. 15(a)]. During late 1998, variations consistent with an orbit period (see Fig. 17(a) between 890 and 1100 days past 1996) start dipping below 30 deg C for significant parts of the orbit period. During several of the experiments conducted during this time, severe degradation was observed, and the cause was confirmed by real-time telemetry to be SSPA temperatures below 30 deg C. This 30 deg C threshold for signal degradation was known from preflight testing data.

**Table 6. MGS/KaBLE-II link advantage, pass 97-232, 80-deg modulation index case.**

Parameter	X-band	Ka-band	Delta, dB
Measured $P_c/N_0$	39.1 dB-Hz	32.6 dB-Hz	-6.5
Power	25 W	1.2 W	13.2
Antenna gain	39 dBi	49 dBi	1.6
Circuit loss	1.0 dB	3.5 dB	2.5
Net EIRP correction	—	—	17.3
Ranging suppression	0.2 dB	3.4 dB	3.2
Telemetry suppression	14.9 dB	2.52 dB	-12.4
LNA temperature <sup>a</sup>	3.2 dB (50 K)	2.1 dB (85 K)	-1.1
Correction to 80 deg	—	5.7 dB	5.7
Net advantage	—	—	6.2

<sup>a</sup>Note that the LNA correction for X-band is  $-10 \log[(T_{op} - 26)/T_{op}]$ , and for Ka-band it is  $-10 \log[(T_{op} - 33)/T_{op}]$ .

**B. MGS Ka-Band/X-Band Solar Corona Experiment (May 1998)**

Data also were acquired when MGS was angularly near the Sun during the period around superior conjunction in May 1998. Because Ka-band signals are less affected by the Sun’s corona than are X-band signals, Ka-band communications should be more easily maintained during solar conjunction. The projected advantage in  $P_c/N_o$  for Ka-band over X-band (see Section V.A) during the solar-corona period is displayed in Fig. 19. The observed increased Ka-band link advantage (Fig. 19) over that observed during normal cruise [Fig. 18(a)] is apparent and is due to the increased degradation of the X-band signal, which in turn is attributed to the effects of spectral broadening and angular broadening. The significantly increased X-band noise temperature due to the solar corona and the wider ground-antenna beamwidth significantly reduced the ETT detection threshold when the spacecraft was angularly near the Sun. This, in turn, required loop bandwidth settings that were narrower than the broadened carrier-signal spectrum at X-band.

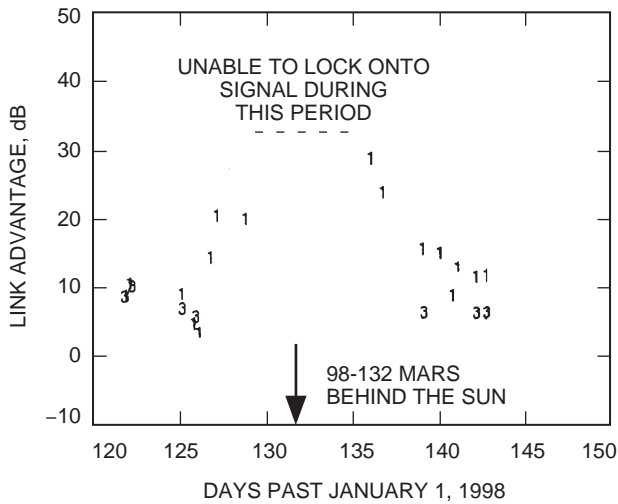


**Fig. 19. Ka-band link advantage versus day of year for solar corona passes in May 1998.**

The Ka-band data acquired during this period also were transferred to Signal Processing Center (SPC 10) via fiber optics for radio science experiments that measure scintillation effects and remote probing of the solar corona.

### C. Frequency-Data Analysis Results

This subsection reports on the X-band and Ka-band frequency data acquired by the ETT during MGS cruise for passes conducted during 1997 through 1998 when the spacecraft Ka-band downlink was purely coherent with the X-band downlink.

Frequency residuals for the individual bands were computed by STBLTY by removing a model frequency from each observable frequency at each time tag. Trajectory files, produced by the MGS Navigation Team, were available in SPICE kernel form. These files were used to steer the frequency data into individual frequency-band residuals for both X-band and Ka-band. A troposphere correction also was applied. Typical frequency residuals for the individual frequency bands are displayed in Fig. 20(a) for X-band and Fig. 20(b) for Ka-band for pass 97-002 conducted on January 2, 1997. Evident upon inspection of these residuals are significant systematic trends (sinusoidal signatures). These trends are believed to be due to dynamic motion of the spacecraft that is not modeled in the trajectory (spacecraft spin, etc.). This pass was the first pass in which the Ka-band data were emitted by the spacecraft's HGA when the Earth passed within the center of the beam (not yet Earth fixed). The received Ka-band signal-to-noise,  $P_c/N_o$ , was at its strongest level measured (58 dB-Hz averaged over the pass). The X-band signal strength (which usually is stronger) was much weaker (46 dB-Hz) since the X-band was on the low-gain antenna (LGA) for this pass.

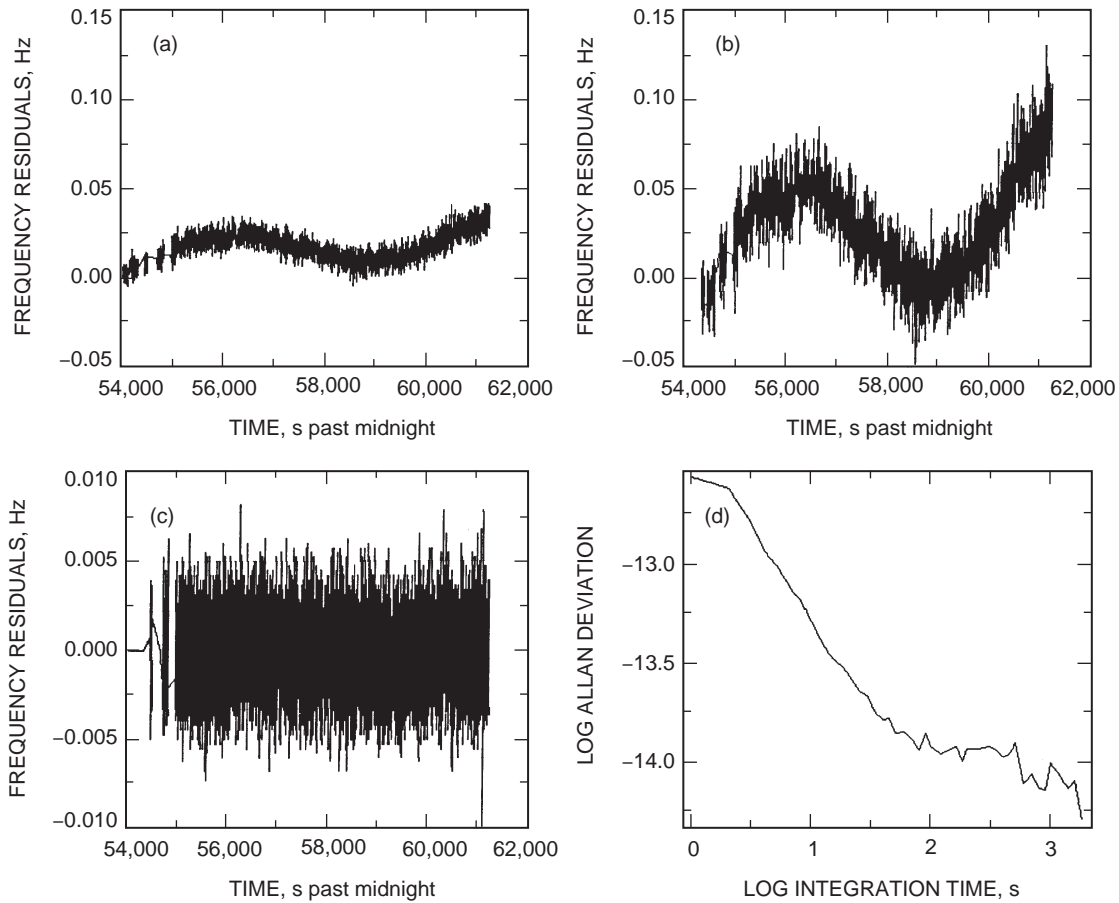


Fig. 20. 97-002 (a) X-band frequency residuals, (b) Ka-band frequency residuals, (c) difference frequency residuals, and (d) Allan deviation of difference frequency residuals of Fig. 20(c).

Table 7 summarizes the Allan deviations  $\sigma_y(\tau)$  for  $\tau = 1, 10, 100$ , and  $1000$  s for both the X-band and Ka-band frequency residuals. Also in Table 7, for comparison, are the preflight USO Allan deviation measurements, which should agree with the individual band values when other effects do not dominate. The X-band and Ka-band Allan deviations are in good agreement with each other for  $\tau = 10, 100$ , and  $1000$  s but are higher than expected preflight values for the USO. The higher values presumably are due to unmodeled spacecraft motion as exemplified in the trends seen in Figs. 20(a) and 20(b). The 1-s Allan deviations are believed to be dominated by a combination of nearly equal contributions of thermal noise and the USO.

**Table 7. Allan deviation summary for 97-002.**

$\tau$ , s	X-band $\sigma_y(\tau) \times 10^{13}$	Ka-band $\sigma_y(\tau) \times 10^{13}$	USO preflight $\sigma_y(\tau) \times 10^{13}$	$X - Ka/3.8$ $\sigma_y(\tau) \times 10^{13}$
1	3.10	1.83	1.2	2.68
10	1.91	1.84	0.64	0.51
100	1.40	1.21	0.72	0.12
1000	5.65	5.34	0.89	0.10

Thus, the frequency residuals estimated for individual frequency bands are dominated by a combination of thermal noise, the USO (when in the one-way mode), and unmodeled dynamic spacecraft motion in the form of significant systematic trends.

For the passes when Ka-band is coherent with X-band, the received downlink Ka-band frequency is an exact factor of 3.8 times the X-band received frequency. By taking frequency differences across identical time tags of the form  $f_X - f_{Ka}/3.8$ , all nondispersive error contributions, including unmodeled dynamic spacecraft motion, cancel out in the resulting difference residuals. The remaining noise sources should include thermal noise (significant at small time scales) and charged particles (which dominate at higher time scales). The difference frequency residuals are effectively a measure of the charged-particle effect on the X-band link since the effect at Ka-band is significantly smaller (by the ratio of the frequencies squared). The resulting frequency differences in Fig. 20(c) for pass 97-002 clearly display a significantly cleaned and flattened residual plot [note the difference in frequency scale with that in Figs. 20(a) and 20(b)]. The corresponding Allan deviation plot for these frequency differences is provided in Fig. 20(d), and the individual values at 1, 10, 100, and 1000-s time intervals are listed in the last column of Table 7.

The corresponding results for pass 97-017 (January 17, 1997) are displayed in Fig. 21(a) (X-band residuals), Fig. 21(b) (Ka-band residuals), Fig. 21(c) (difference frequency residuals), and Fig. 21(d) (Allan deviation of difference frequency residuals). Table 8 summarizes the Allan deviation results for pass 97-017. Note that the individual-band Allan deviations are in better agreement with the USO preflight values, but that unmodeled spacecraft motion still contributes at the higher time intervals, especially at 1000 s. The troposphere contributes noise to the individual-band Allan deviations, but it cancels out in the difference frequency and, thus, its effect is removed in the difference-frequency Allan deviations along with all other nondispersive noise sources. The X-band signal strength (56 dB-Hz) and Ka-band signal strength (53 dB-Hz) were comparable for this pass. The difference-frequency residual Allan deviations for 10, 100, and 1000 s significantly exceed predicted estimates based on SNR thermal noise and, thus, are attributed to charged-particle effects on the X-band link.

For all of the KaBLE-II passes conducted for which significant time periods of coherent X-band and Ka-band data were acquired, the Allan deviations of the difference data type ( $f_X - f_{Ka}/3.8$ ) were estimated for time intervals of 1, 10, 100, and 1000 s. Figures 22(a) through 22(d) display the Allan deviation versus day number for time intervals of 1, 10, 100, and 1000 s, respectively. The “+” symbols in Figs. 22(a)

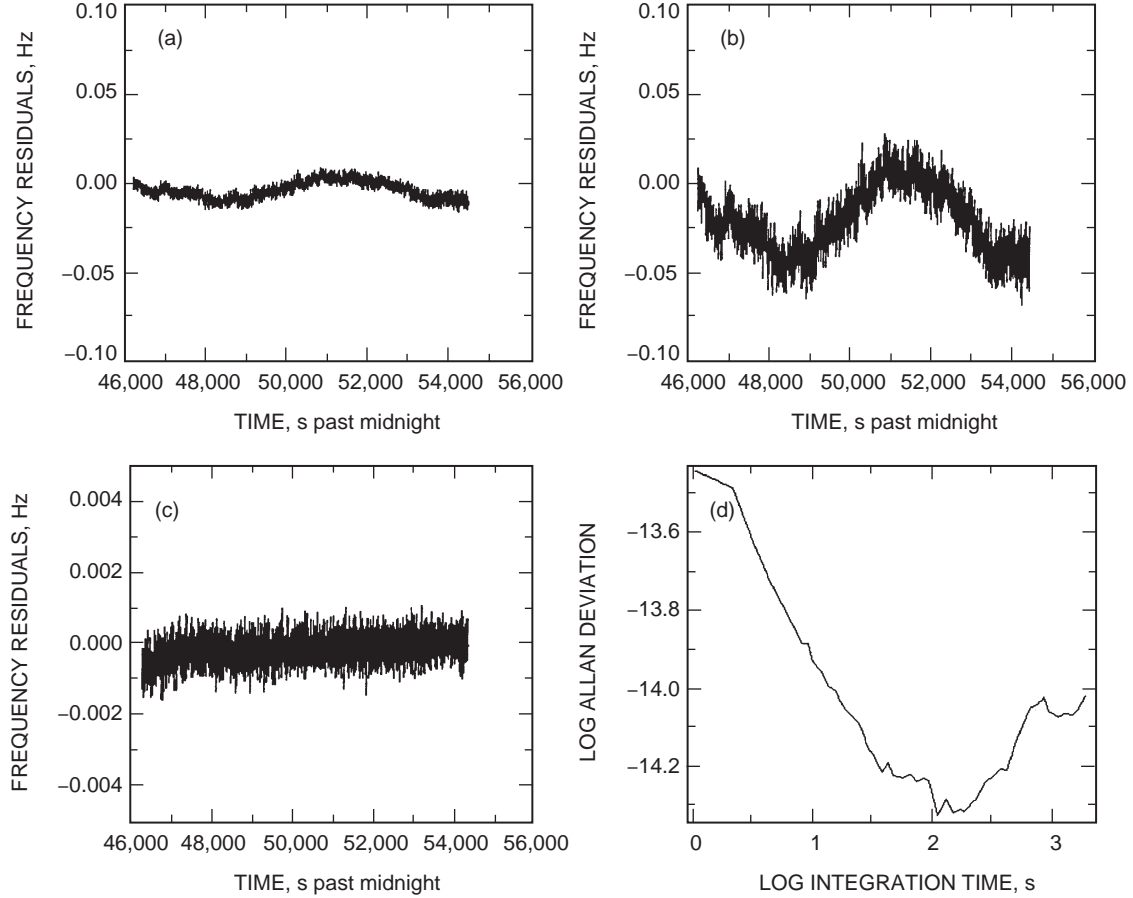


Fig. 21. 97-017 (a) X-band frequency residuals, (b) Ka-band frequency residuals, (c) difference frequency residuals, and (d) Allan deviation of difference frequency residuals of Fig. 21(c).

Table 8. Allan deviation summary for 97-017.

$\tau$ , s	X-band $\sigma_y(\tau) \times 10^{13}$	Ka-band $\sigma_y(\tau) \times 10^{13}$	USO preflight $\sigma_y(\tau) \times 10^{13}$	$X - Ka/3.8$ $\sigma_y(\tau) \times 10^{13}$
1	1.15	1.11	1.2	0.36
10	1.01	1.00	0.64	0.12
100	0.96	0.97	0.72	0.06
1000	3.91	3.93	0.89	0.09

through 22(d) denote actual measurements. The Allan deviation for the shorter time intervals generally were in agreement with the predictions based on thermal noise. The 1000-s Allan deviations are shown in Fig. 23 as a function of solar elongation angle. A general trend is apparent that shows Allan deviation decreasing as solar elongation angle increases from near 6 deg to about 170 deg. This trend is reasonably consistent with a model curve presented elsewhere for S-band frequency data [11]. The expected thermal noise contributions to the 1000-s Allan deviations lie well below the observed Allan deviations. The observed 1000-s Allan deviations are consistent with expected solar plasma effects on the X-band link. The majority of the 1000-s Allan deviations shown clustered at high solar elongation angles in Fig. 23 (above 160 deg) are in good agreement with a predicted Allan deviation value ( $6 \times 10^{-15}$ ) for the antisolar direction at X-band [11].

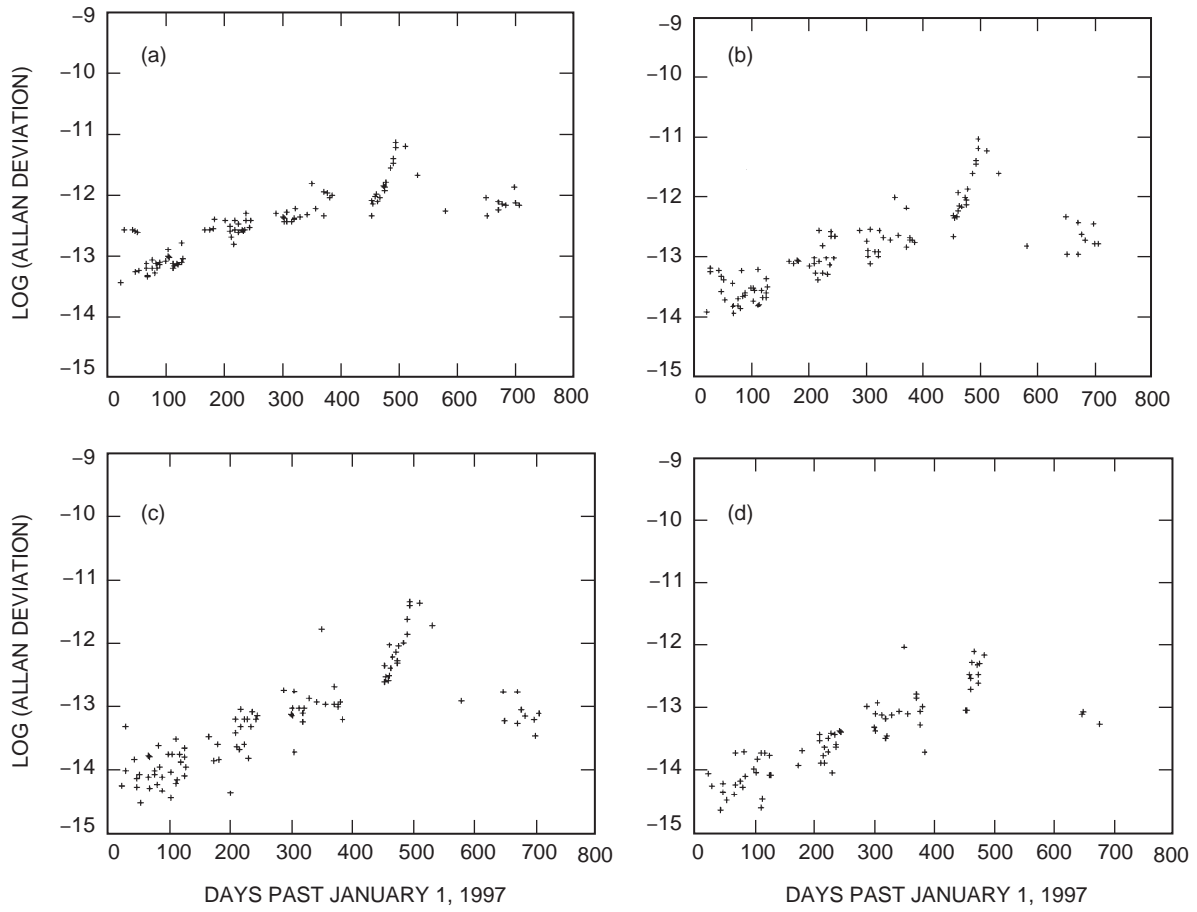


Fig. 22. Allan deviations ( $\sigma_y(\tau)$ ) versus day of year: (a)  $\tau = 1$  s, (b)  $\tau = 10$  s, (c)  $\tau = 100$  s, and (d)  $\tau = 1000$  s.

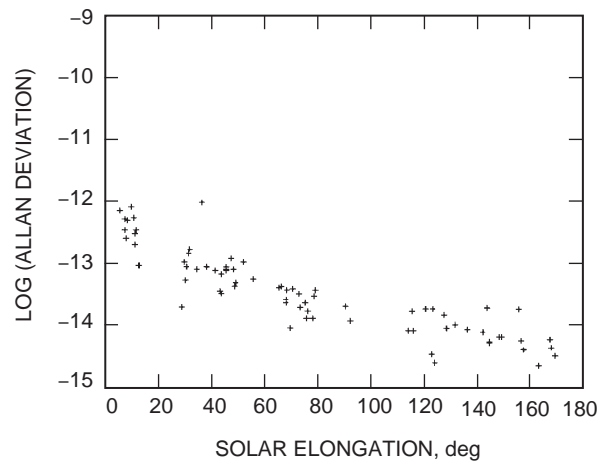


Fig. 23.  $\tau = 1000$  s Allan deviations versus solar elongation angle.

## D. Telemetry Demonstration

An end-to-end Ka-band telemetry demonstration was conducted from April 14 through May 2, 1997. The Mars Surveyor Operations Project (MSOP) received and displayed telemetry transmitted at 2 kb/s by MGS over its experimental Ka-band link as well as over its operational X-band link. Figure 24 shows the monitor terminal displaying plots of spacecraft engineering data as received on both frequencies. There were no errors as both links were significantly above margin.

The Ka-band radio signal was received at DSS 13 while DSS 15 provided the operational X-band uplink and downlinks, as depicted in Fig. 25. Both the X-band downlink from DSS 15 and the Ka-band downlink from DSS 13 were downconverted to IF and cabled over to SPC 10 for telemetry and radio metric processing and delivery to the project database. Dual-frequency ranging data also were obtained at Ka-band and X-band. The projected 5- to 6-dB advantage of Ka-band over X-band using received  $E_b/N_o$  measurements is shown in Fig. 26. The measurements were converted to projected advantage assuming equivalent X-band and Ka-band equipment specifications and projected X-band LNA temperature performance.

## E. Ranging-Data Demonstration

The system configuration for MGS simultaneous Ka-band and X-band ranging utilized the operational DSN station, DSS 15, which provided the X-band uplink signal and received the X-band downlink. This is the standard operational two-way ranging configuration with the spacecraft. The R&D station, DSS 13, which was in the listen-only mode, tracked the Ka-band signal, downconverted it to 300-MHz IF, and then sent it through optical fiber to the BVR located in the main Goldstone complex, SPC 10. This configuration uses the DSS-13 front-end to track the Ka-band downlink; however, data demodulating, processing, and formatting all are performed by DSN operational equipment. The two receiver channel processors (RCP 1 and 2), part of the BVR of DSS 15, simultaneously demodulated DSS-13 Ka-band IF on RCP 1 and DSS-15 X-band IF on RCP 2. Ranging baseband correlation was performed by the sequential ranging assembly (SRA). The metric data assembly (MDA)-formatted radio metric data (including ranging data) were sent to the navigation subsystem for processing. The data used in the analysis were extracted from a computer server that stores the files forwarded by the Navigation Team.

The ranging experiment conducted during 97-107 and 97-108 will now be described.<sup>8</sup> The ranging-power-to-noise values,  $P_r/N_o$ , as measured by the SRA are comparable, as expected. The X-band link has about 12 dB more total power to noise ( $P_t/N_o$ ) than does Ka-band; however, the X-band ranging modulation index is only 12.2 deg, while at Ka-band it is multiplied by 4 to 50 deg. This makes  $P_r/P_t$  11-dB greater at Ka-band. Table 9 presents the average measured  $P_r/N_o$ , the standard deviation (sigma) of the residual plots, and the computed sigma based on the thermal noise model, which uses the average measured ranging channel,  $P_r/N_o$ , and the actual integration time,  $T_1 = 20$  s.

Range residuals on each SRA channel for pass 97-108 are given in Fig. 27. The residuals shown are what remains after a 6th order polynomial curve is fit to each data set separately. The residuals at Ka-band are about 4 times as large as those at X-band. This may have been caused by a deteriorating circuit card in the SRA, which was discovered and replaced several weeks later following tests with Mars Pathfinder. A retest was conducted on 97-224 and 97-225, and the results are depicted in Fig. 28. Here the Ka-band ranging scatter lay below the X-band ranging scatter, consistent with the SNR. Thus, X-/Ka-band simultaneous ranging using DSN operational equipment was demonstrated successfully.

---

<sup>8</sup> A. Kwok, "Mars Global Surveyor (MGS) Ka- and X-Band Ranging Data Analysis," JPL Interoffice Memorandum 3315-97-AK-104 (internal document), Jet Propulsion Laboratory, Pasadena, California, May 15, 1997.

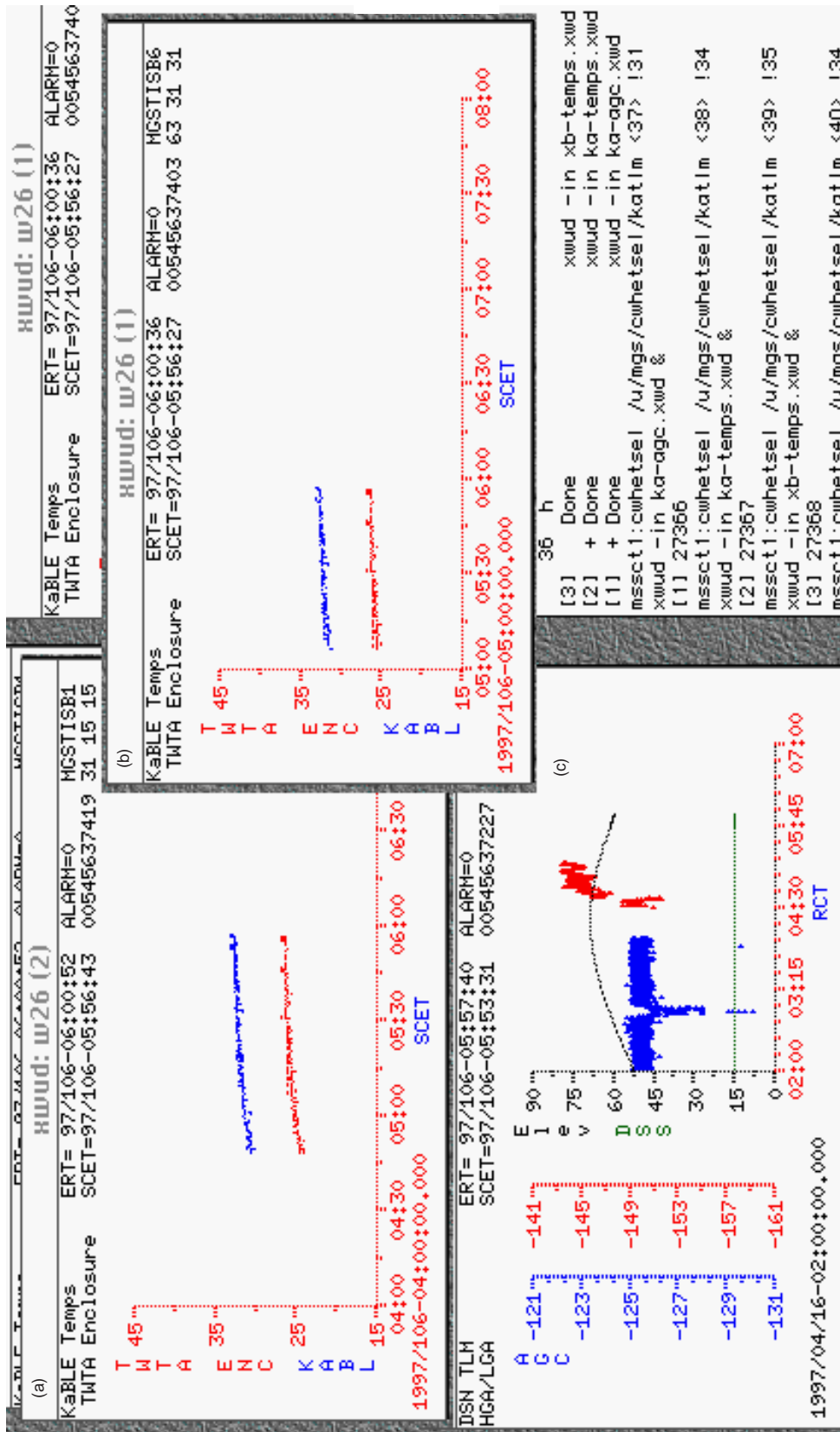


Fig. 24. Monitor terminal display plots for MGS X-band/Ka-band telemetry data: (a) spacecrafft engineering telemetry received via Ka-band at DSS 13, (b) the same engineering telemetry received via X-band at DSS 15, and (c) signal levels at X-band (blue scale) and Ka-band (red scale); improved during warm up).

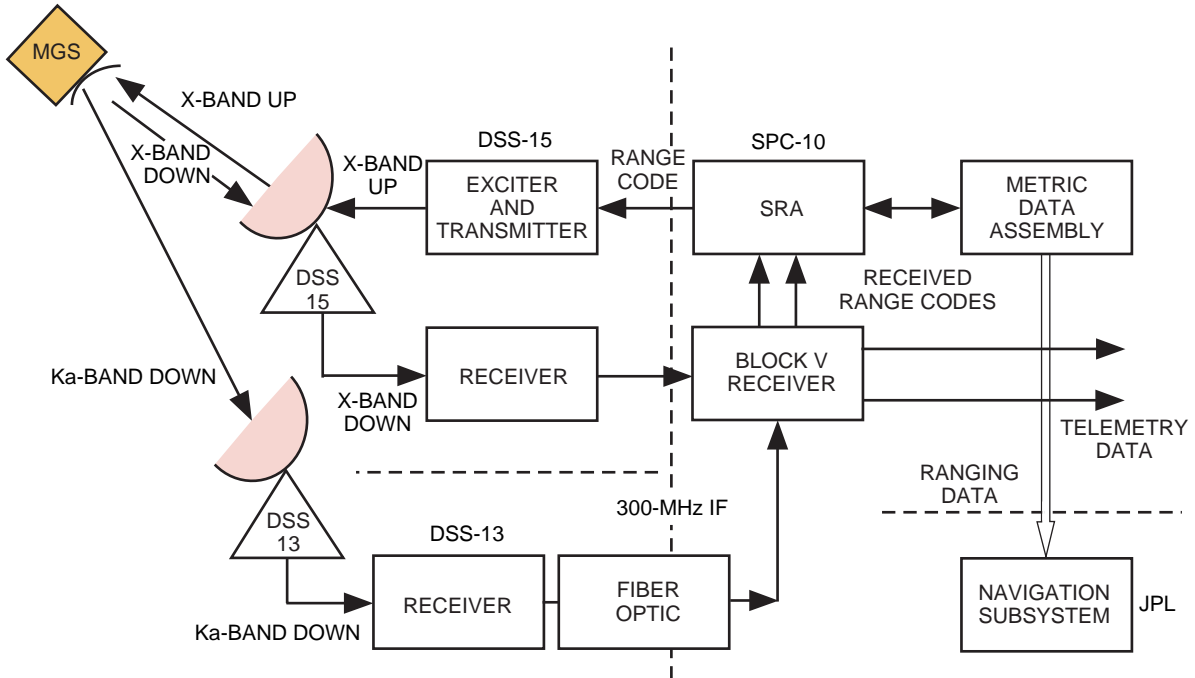


Fig. 25. DSS-13/DSS-15 telemetry demonstration.

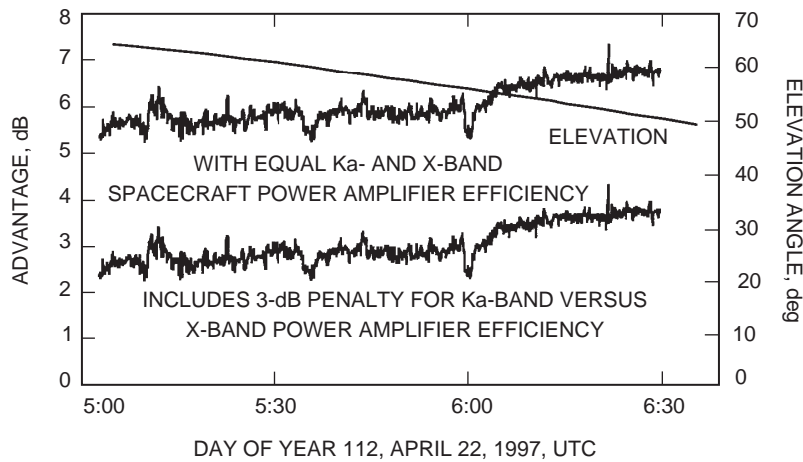


Fig. 26. MGS/KaBLE-II telemetry results demonstrating a 5- to 6-dB Ka-band advantage from  $E_b/N_0$  measurements.

## VI. Conclusion

The MGS/KaBLE-II link experiment (1) measured signal strengths that were in general agreement with predicted values, (2) measured frequency residuals that were in agreement between bands and whose statistics were consistent with expected noise sources, (3) acquired range data that demonstrated Ka-band ranging, and (4) delivered telemetry in real time to the MGS project that was validated by simultaneously received X-band telemetry data used by the MGS Project. The relative performances of X-band and

Ka-band over an extended period will continue to be quantified as additional data are acquired under a wide range of elevation angles and atmospheric conditions. There are, as alluded to in several places before, many variables that need to be understood and controlled at both ends of the link before Ka-band operation becomes routine and predictable. These efforts had continued in 1999 with MGS/KaBLE-II as well as with DS1, which was launched in October 1998.

**Table 9. Ranging demonstration summary.**

Day of year	Frequency band	Average $P_r/N_o$ , dB-Hz	Residual sigma, <sup>a</sup> RU	Computed sigma, <sup>a</sup> RU
97-107	Ka-band	33.2	7.4	0.7
97-107	X-band	33.8	1.8	0.7
97-108	Ka-Band	32.1	9.3	0.8
97-108	X-band	33.4	2.0	0.7

<sup>a</sup>The range unit (RU) is related to the transmitting (uplink) frequency,  $F_{tx}$ , of DSS 15 by  $1 \text{ RU} = 1/(16 \times 11 \times F_{tx}/1200)$ . For 97-107,  $1 \text{ RU} = 0.951601871 \text{ ns}$ ; for 97-108,  $1 \text{ RU} = 0.951601611 \text{ ns}$ .

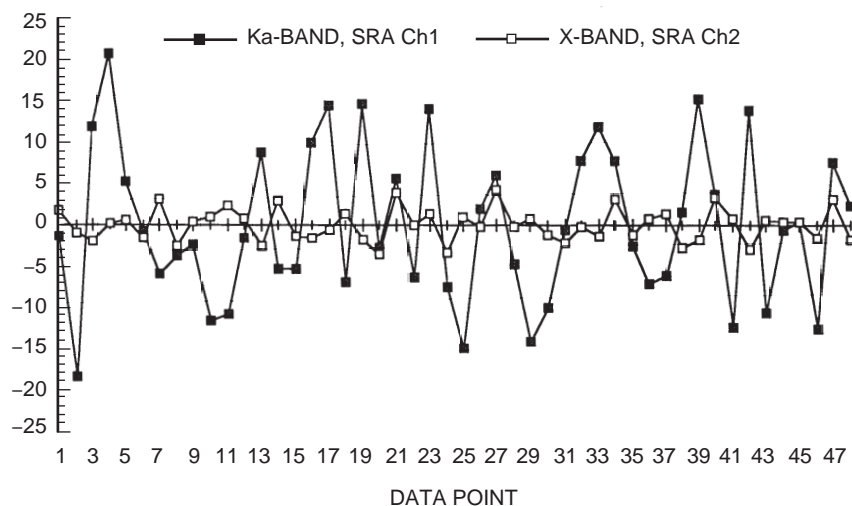


**Fig. 27. X-band and Ka-band range residuals for 97-108.**

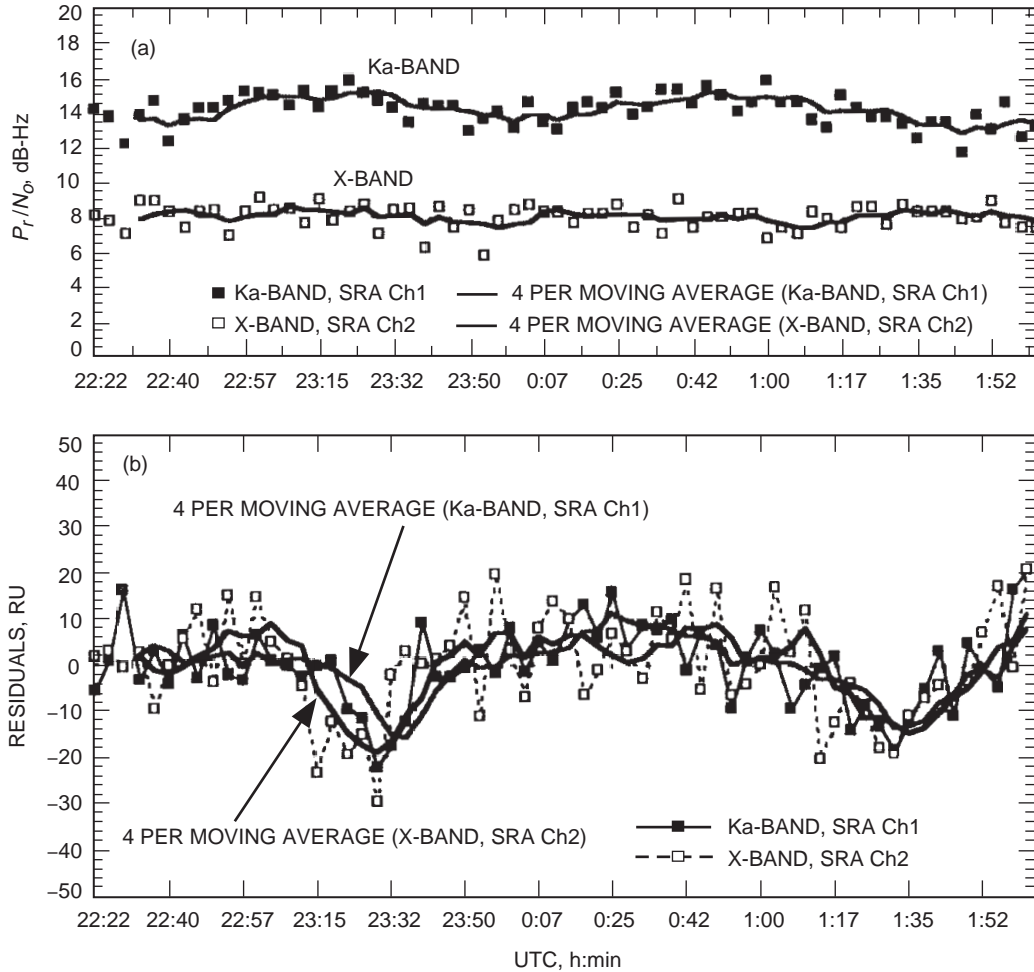


Fig. 28. X-band and Ka-band range residuals for 97-224/225: (a)  $P_r/N_0$  measurements and moving averages and (b) range residuals and curve fits.

## Acknowledgments

We would like to thank J. Beerer, G. Cunningham, L. Deutch, C. Edwards, R. Horttor, W. Lee, C. Mcannaly, G. Pace, W. Rafferty, C. Stelzried, T. Yan, J. Yuen, S. Portas, and H. Fosque for their support, guidance, and continuing interest in this work; the DSS-13 station personnel for conducting the experiments (C. Goodson, G. Bury, J. Crook, G. Farner, J. Garnica, R. Littlefair, R. Reese, and L. Smith); J. McCluskey, L. Teitelbaum, and P. Wolken for scheduling support; M. Ryne for navigation support; the MSOP Sequence and Spacecraft Operation Teams at JPL (A. Mittskus, J. Border, J. Berner, C. Whetsel, M. Gatti, and C. Foster); L. Skjerve, L. Tanida, V. Vilnrotter, R. Clauss, T. Rebold, H. Cooper, A. Del Castillo, A. Kwok, J. Weese, and D. Recce for their technical expertise and assistance; R. Davis, W. Adams, A. McMechen of Lockheed-Martin Astronautics Co. (LMA); J. Caetta for computational consulting assistance; M. Speranza, T. Buckley, L. Moreno, and A. Milanian for assistance in data processing; and T. Priest and the MGS Navigation Team for providing trajectory files.

## References

- [1] W. R. Corliss, *History of the Deep Space Network*, NASA Report CR-151915, National Aeronautics and Space Administration, May 1, 1976.
- [2] S. Butman, D. Morabito, A. Mittskus, J. Border, J. Berner, C. Whetsel, M. Gatti, C. Foster, C. Chen, H. Cooper, A. Del Castillo, A. Kwok, J. Weese, M. Speranza, R. Davis, W. Adams, A. McMechen, C. Goodson, G. Bury, and D. Reece, “The Mars Global Surveyor Ka-Band Link Experiment (MGS/KaBLE-II),” *Proceedings of the 3rd Ka-band Utilization Conference*, Sorrento, Italy, November 1997.
- [3] D. D. Morabito, S. Butman, and S. Shambayati, “Recent Results From the Mars Global Surveyor Ka-band Link Experiment (MGS/KaBLE-II),” *Proceedings of the 4th Ka-Band Utilization Conference*, Venice, Italy, November 1998.
- [4] T. A. Rebold, A. Kwok, G. D. Wood, and S. Butman, “The Mars Observer Ka-Band Link Experiment,” *The Telecommunications and Data Acquisition Progress Report 42-117, January–March 1994*, Jet Propulsion Laboratory, Pasadena, California, pp. 1–33, May 15, 1994.  
[http://tmo.jpl.nasa.gov/tmo/progress\\_report/42-117/117u.pdf](http://tmo.jpl.nasa.gov/tmo/progress_report/42-117/117u.pdf)
- [5] T. Milligan, “Compact Dual Band Feed for Mars Global Surveyor,” 1995 IEEE AP-S International Symposium and USNC/URSI Radio Science Meeting, Newport Beach, California, June 18–23, 1995.
- [6] D. D. Morabito, “The Efficiency Characterization of the DSS-13 34-Meter Beam-Waveguide Antenna at Ka-Band (32.0 and 33.7 GHz) and X-Band (8.4 GHz),” *The Telecommunications and Data Acquisition Progress Report 42-125, January–March 1996*, Jet Propulsion Laboratory, Pasadena, California, pp. 1–20, May 15, 1996.  
[http://tmo.jpl.nasa.gov/tmo/progress\\_report/42-125/125D.pdf](http://tmo.jpl.nasa.gov/tmo/progress_report/42-125/125D.pdf)
- [7] V. Vilnrotter and B. Iijima, “Analysis of Array Feed Combining Performance Using Recorded Data,” *The Telecommunications and Data Acquisition Progress Report 42-125, January–March 1996*, Jet Propulsion Laboratory, Pasadena, California, pp. 1–13, May 15, 1996.
- [8] V. Y. Lo, “Ka-Band Monopulse Antenna-Pointing Systems Analysis and Simulation,” *The Telecommunications and Data Acquisition Progress Report 42-124, October–December 1995*, Jet Propulsion Laboratory, Pasadena, California, pp. 104–112, February 15, 1996.  
[http://tmo.jpl.nasa.gov/tmo/progress\\_report/42-124/124F.pdf](http://tmo.jpl.nasa.gov/tmo/progress_report/42-124/124F.pdf)
- [9] D. D. Morabito and S. W. Asmar, “Radio Science Performance Analysis Software,” *The Telecommunications and Data Acquisition Progress Report 42-120, October–December 1994*, Jet Propulsion Laboratory, Pasadena, California, pp. 121–152, February 15, 1995.  
[http://tmo.jpl.nasa.gov/tmo/progress\\_report/42-120/120B.pdf](http://tmo.jpl.nasa.gov/tmo/progress_report/42-120/120B.pdf)
- [10] W. H. Press, B. P. Flannery, S. A. Teukolsky, and W. T. Vetterling, *Numerical Recipes, the Art of Scientific Computing*, New York: Cambridge University Press, 1986.
- [11] J. W. Armstrong, R. Woo, and F. B. Estabrook, “Interplanetary Phase Scintillation and the Search for Very Low Frequency Gravitational Radiation,” *The Astrophysical Journal*, vol. 230, pp. 570–574, June 1, 1979.